Bolides in the present and past martian atmosphere and effects on cratering processes

Olga POPOVA,[1][*] Ivan NEMTCHINOV,[1] and William K. HARTMANN[2]

[1]Institute for Dynamics of Geospheres, Russian Academy of Sciences, Leninsky Prospekt 38, Building 1, 119334, Moscow, Russia
[2]Planetary Science Institute, 620 North 6th Avenue, Tucson, Arizona 85705, USA
[*]Corresponding author. E-mail: olga@idg.chph.ras.ru

Abstract–We investigate the action of the martian atmosphere on entering meteoroids for present and past atmospheres with various surface pressures to predict the smallest observable craters, and to understand the implications for the size distributions of craters on Mars and meteoroids in space. We assume different strengths appropriate to icy, stone, and iron bodies and test the results against available data on terrestrial bolides. Deceleration, ablation, and fragmentation effects are included.

We find that the smallest icy, stone, and iron meteoroids to hit the martian ground at crater forming speeds of ≥500 m/s have diameters of about 2 m, 0.03–0.9 m (depending on strength), and 0.01 m, respectively, in the current atmosphere. For hypothetical denser past atmospheres, the cutoff diameters rise. At a surface pressure of 100 mb, the cutoff diameters are about 24 m, 5–12 m, and 0.14 m for the 3 classes. The weaker stony bodies in the size range of about 1–30 m may explode at altitudes of about 10–20 km above the ground.

These figures imply that under the present atmosphere, the smallest craters made by these objects would be as follows: by ice bodies, craters of diameter (D) ~8 m, by stones about 0.5–6 m, and by irons, about 0.3 m. A strong depletion of craters should, thus, occur at diameters below about 0.3 m to 5 m. Predicted fragmentation and ablation effects on weak meteoroids in the present atmosphere may also produce a milder depletion below D ~500 m, relative to the lunar population. But, this effect may be difficult to detect in present data because of additional losses of small craters due to sedimentation, dunes, and other obliteration effects. Craters in strewn fields, caused by meteoroid fragmentation, will be near or below present-day resolution limits, but examples have been found.

These phenomena have significant consequences. Under the present atmosphere, the smallest (decimeter-scale) craters in sands and soils could be quickly obliterated but might still be preserved on rock surfaces, as noted by Hörz et al. (1999). Ancient crater populations, if preserved, could yield diagnostic signatures of earlier atmospheric conditions. Surfaces formed under past denser atmospheres (few hundred mbar), if preserved by burial and later exposed by exhumation, could show: a) striking depletions of small craters (few meter sizes up to as much as 200 m), relative to modern surfaces; b) more clustered craters due to atmospheric breakup; and c) different distributions of meteorite types, with 4 m to 200 m craters formed primarily by irons instead of by stones as on present-day Mars. Megaregolith gardening of the early crust would be significant but coarser than the gardening of the ancient lunar uplands.

BACKGROUND: SIZE DISTRIBUTION OF SMALL CRATERS ON MARS

On each planetary body, the smallest craters (D <1 km) offer a special challenge. In the 1960s, the Ranger probes returned the first close-up image of craters on another world, revealing a steep upturn in the size distribution from −1.8 slope to about −3 to −3.5 slope. To explain this, Shoemaker (1965) and others counted secondary craters around several larger lunar craters and found the same steep −3 to −3.5 slope.

From this, Shoemaker (1965) concluded that the steep branch was due to secondary debris being thrown out of lunar craters and falling back on the lunar surface. Neukum and Ivanov (1994) found moderate crater densities with a steep branch (slope ~−3.4) among craters of 200 m <D <1 km on asteroid Gaspra, showing that the steeply upturned branch is not just a consequence of lunar secondary debris alone but is present in the population of interplanetary bodies. It may be thought of as the cumulative result of the "secondaries" thrown out of craters on the whole population of asteroids.

The steep slope of the size distribution among small bodies implies large numbers of them hitting planetary bodies, consistent with the rain of meter-scale and sub-meter-scale meteorites entering the earth's atmosphere. Shoemaker (1965), thus, hypothesized that the extremely large numbers of small impactors create a gardening effect that fragmented the lunar surface layers and produced a roughly 10 m deep layer of a regolith since the lunar maria formed. This explanation of regolith has been generally accepted.

The earth's atmosphere causes dramatic breakup and loss of small bolides and small craters. The luminous and explosive phenomena of meteoroids passing through atmospheres lead to some confusion of nomenclature. Here, we follow the *Encyclopedia of Astronomy and Astrophysics* (Murdin 2001) in noting that "meteoroid" generally refers to relatively small debris (sub-meter scale in some usages and tens of meters in others) in interplanetary space that enters atmospheres; "meteor" refers to the "transient luminous phenomena visible in the night sky" and generally implies small meteoroids; and "bolide" refers to "a bright meteor" that can involve explosions and meteorite fragments. The objects that create the smallest martian craters are generally in the latter size range and would be perceived from the martian surface as bolides. We will refer to them as meteoroids or, in recognition of the atmospheric effects, bolides.

Mars presents an intermediate situation between the lunar and Earth cases. On Mars, the effects of meter and sub-meter scale impactors have received surprisingly little attention, partly for historical reasons. Early flyby and orbiter missions rarely resolved features much below 100 m in scale. Most workers assumed qualitatively that the atmosphere blocked modest-scale bolides so that there would be no equivalent to the finely gardened lunar regolith. This assumption was made more quantitative by Gault and Baldwin (1970), who predicted that the atmosphere would break up meteoroids of a size sufficient to make craters of diameter (D) <50 m.

Another problem in the literature on small craters is that the sub-km crater population was not widely studied because researchers focused on comparisons at multi-km scales between crater populations on Mars and the outer planet satellites imaged by Voyagers 1 and 2 during the 1980s, where sub-km craters were usually not resolved. Furthermore, Tanaka (1986) defined the martian stratigraphic column (the Noachian-Hesperian-Amazonian eras) only in terms of crater densities at scales of D = 1 to 20 km. Thus, for example, the major review article on martian cratering by Strom et al. (1992) contained no crater count data on any martian craters smaller than 4 km even though Viking orbiters 15 years earlier had shown craters down to the 100 m and less.

Starting in the early 1990s, several workers began to reassess small scale martian cratering. Padevět (1991) used classical theory of meteors (Bronshten 1983) and predicted penetration depths for various types of chondrites with weights in excess of 0.1 kg. His strength value for the strongest chondrites was much higher than realistic. Nemtchinov and Shuvalov (1992) estimated the sizes of the smallest bolides hitting the surface of Mars at hypervelocity and estimated meteoroid diameters of 3 cm and 10 cm for stones and icy bodies, respectively, suggesting that the cutoff of smallest impact craters on Mars should be of the order 0.5 to 2 m. Vasavada et al. (1993) improved the treatment of deceleration of bolides by various atmospheres with time-varying properties. Independently, Hartmann et al. (1994) and Hartmann and Engel (1994) attempted estimates of the fragmentation during bolide/atmosphere interaction with the present and past martian atmospheres. Their main interest was the atmosphere pressure needed to disrupt various taxonomic types of meteoritic bolides, and they concluded that at pressures above a few hundred mbar, smaller stony and icy meteorites would break up, leaving only craters caused by irons at sizes below about 0.5 to 4 km. Their additional unpublished results were consistent with modern-day craters down to about 1 m diameter, from both stony and iron bolides, under the current atmosphere. Meanwhile, Rybakov et al. (1997) and Nemtchinov et al. (1998, 1999a) suggested that small impactors may eject large amounts of dust into the martian atmosphere and may even create local dust storm conditions.

In 1997–98, Mars Global Surveyor (MGS) first revealed a population of impact craters that appears relatively complete down to D <11 m (Malin et al. 1998; Hartmann et al. 1999), a finding not inconsistent with the above calculations. The new data require a careful investigation of the smallest bolides hitting the martian surface at hypervelocity (usually defined as >speed of sound in target materials) because such impactors may have substantial effects. For example, Hörz et al. (1999) pointed to an example of a possible meteorite-caused spall at 0.2 m scale on a rock in the Pathfinder lander images. In principle, this could have been caused by a hypervelocity meteorite or by a larger fragment from a breakup event falling at a speed more like terminal velocity. Hörz et al. (1999) also modeled martian atmospheric passage of small meteoroids, taking into account ablation and drag, but they did not take into account fragmentation (see below). Precise estimates of the smallest impactors are important because the size distribution of small meteoroids increases at a steep rate toward small diameters, and this means that a small decrease in the size of the smallest impactors has a large effect in the number density of impacts and the timescale on which surfaces can be degraded by impact gardening.

This is not to say that wind transport, fluvial, and other erosional processes do not dominate surface conditions but, rather, that small impacts could have additional consequences. An interplay, which depends on timescales, exists between the exogenic and endogenic processes. For example, if an ancient fluvial episode left a lakebed deposit of carbonates and salts 1 cm thick, and if the timescale for impact gardening and erosion is much less than the likely

characteristic timescale for burial and preservation by windblown dust, then such deposits would likely have been broken up and diluted beyond MGS spectroscopic recognition before they could be covered and preserved.

Hartmann et al. (2001) examined martian gardening effects from the known crater statistics. Strictly on geometric grounds of total areal crater coverage, and independent of any models of time dependent impact fluxes, he concluded that mid-Hesperian surfaces have experienced coarse gardening to a depth of some meters and Noachian surfaces to a depth of tens of meters or (for the early Noachian) even hundreds of meters. The idea of coarse gardening is independent of the cutoff size of the smallest martian bolides because 100% of the surface area, in regions older than mid Hesperian, has been excavated by observable craters of D = 50 m. However, the meteoroid cutoff size will determine the degree of fine-scale gardening and erosion of rock surfaces, and this needs to be better determined. Hartmann noted, for example, that preservation of thin, intact Noachian/Hesperian lakebed deposits would require burial during part or all of their history to protect them from the postulated gardening effects. A few rare examples of such preserved surfaces may have been recently exhumed, such as the Meridiani Terra hematite-rich surface (Christensen et al. 2000; Hartmann 2001). This study also noted that if the cutoff of smallest hypervelocity impact craters is close to diameter (D) = 1 m in size, then martian surfaces with crater densities less than ~1% of lunar mare crater densities (tens of Myr age, possibly found among the youngest lava flows) would have negligible impact gardening because even the smallest impacts would not saturate the surface.

Due to oscillating obliquity (Ward 1992), Mars' atmosphere may vary over a modest range of surface pressures. The martian obliquity varied by as much as ~±20° and is characterized by 10^5-yr oscillations supplemented by 10^6-yr modulation of its amplitude (Ward 1992). These oscillations cause variation of atmosphere density due to changes in insolation and ice stability. In principle, the record of impact cratering could show evidence of the historical behavior of such changes in the planet atmosphere.

Thicker transient atmospheres may also be produced for a significant period of time by extensive volcanism on Mars. Pollack et al. (1987) proposed that an early, wet martian climate was sustained by a thick CO_2 atmosphere, and that extensive volcanism was the mechanism of CO_2 recycling. Analysis of MGS images led to a conclusion by McEwen et al. (1999) that volcanism on early Mars was probably much more voluminous than previously documented and that it must have affected the climate and near-surface environment. Moreover, martian rocks and crater counts provide evidence for voluminous volcanism in the last quarter of martian history (Nyquist et al. 2001; Hartmann et al. 1999; Hartmann and Neukum 2001). MGS images show fresh lava flows with crater count model ages less than 100 Myr (Hartmann 1999;

Hartmann and Neukum 2001). Thus, the past martian atmospheric pressure has not necessarily been fixed at its current value.

New observations of atmospheric passage of relatively big terrestrial meteoroids (1–10 m) allow more rigorous treatment of martian bolides and understanding of small craters. In particular, many of these bolides (including the stones) were found to be weaker than previously assumed and are disrupted in the earth's atmosphere at altitudes of 25–40 km. In the current martian atmosphere, some of these bodies should be severely fragmented below an altitude of 15 km and reach the surface as a swarm of fragments (Nemtchinov et al. 1999b). Based on the above ideas, we have set the following goals for this paper:

- Use modern modeling of bolide fragmentation to determine the size of the smallest hypervelocity bolides to reach the martian surface under current atmospheric conditions.
- Derive this result for each major meteoritic compositional class, ranging from weakly consolidated carbonaceous and/or icy (cometary?) bodies through ordinary chondritic rocks to coherent iron meteorites. We note that the smallest objects to survive will be irons (as on Earth).
- Because irons constitute only a few percent of all meteoroids, investigate the offset in the crater diameter distribution that should appear at the size reflecting breakup and loss of the chondritic rock impactors, with the diameter distribution of craters due to irons extending to smaller diameters, but at only a few percent of the density at larger sizes.
- Determine the same sets of results for hypothetical past martian atmospheres.
- Study the disruption phenomena for fragmenting bolides and examine the question of the origin of martian crater clusters pointed out by Hartmann and Engel (1994).

CRATER DIAMETER SCALING LAW AND METEOROID VELOCITY DISTRIBUTION

To study effects of atmosphere shielding, we must take into account the efficiency of cratering at different impact velocities. A number of crater energy-diameter scaling laws can be found in Melosh (1989). The most widely used scaling law was proposed by Schmidt and Housen (1987) and may be written as

$$D = 1.16(\rho_m/\rho_t)^{1/3}D_p^{0.78}(V\sin\theta)^{0.43}g^{-0.22} \qquad (1)$$

where D is the crater diameter (in m), D_p is the meteoroid diameter (in m), ρ_m and ρ_t are meteoroid and target densities, V and θ are meteoroid velocity (in m/s) and angle from the horizontal, and g is the gravity acceleration (3.74 m/s² for Mars). According to Christensen and Moore (1992), the bulk

density of martian surface materials is about 1.2–2.6 g/cm³, and we will assume $\rho_t = 2$ g/cm³ here and below.

We assume Equation 1 between crater and projectile sizes may be used if the terminal velocity (V_t) ≥0.5 km/s, and we define this as the cutoff speed for formation of ordinary impact craters. This speed depends somewhat on surface materials and is not sharply defined. At lower speeds, the bolide falls to the ground and may partially or completely bury itself but does not create an explosion crater. In the limit of the lowest terminal velocities, the "crater" is the size of the meteoroid itself. This is somewhat idealized, but our goal here is to predict approximately the smallest high-speed impactors and the smallest recognizable craters that follow Equation 1. In reality, there will be a transition to smaller, lower velocity pits and rock spalls due to smaller, lower velocity meteoroids. Crater diameter is basically dependent on projectile energy.

The normalized distribution of atmospheric entry velocities at Mars (Bland and Smith 2000; Davis 1993; Flynn and McKay 1990) is taken to be

$$F(V) = 0.0231 \, V \exp\left(-\left[\frac{V - 1.806}{8.874}\right]^2\right) \qquad (2)$$

for V >5 km/s. The mean meteoroid velocity is estimated to be 10.2 km/s, and only a small fraction of bolides has entry velocity in excess of 20 km/s. We assume that all types of meteoroids have the same atmospheric velocity. Higher average velocity of cometary material will result in more dramatic fragmentation of cometary meteoroids.

CRATER DISTRIBUTION

The shielding action of the martian atmosphere will affect the craters' size frequency distribution function (SFD). The SFD has been presented several different ways in the literature. The cumulative distribution is the number of craters/km² (N) with diameter larger than a given diameter (D) per unit area. It has the disadvantage of smoothing data and not emphasizing sharp cutoffs in craters below certain sizes where fragmentation may destroy meteoroids. The differential distribution

$$\frac{dN}{dD}$$

is the number of craters in the diameter range from D to D + δD divided by bin width δD. Another form of SFD presentation is the log-incremental representation with a standard bin width in log D. If D_L and D_R are the left and the right bin boundaries, the standard bin width is $D_R/D_L = \sqrt{2}$. The last two systems show depletions at small sizes better than the cumulative system. The log-incremental distribution has the advantage that power-law segments have the same slope as in the cumulative plot, and it was used by Hartmann and Berman (2000) to develop isochrons giving the martian SFD for different surface ages.

Craters of a given diameter (D) may be formed by the impact of projectiles of somewhat different diameters, depending on the impact velocity and impact angle (θ). Thus, to derive size frequency distribution of craters, we sum the number of all projectiles with all possible velocities and angles of impact. In differential form, this condition is expressed as

$$\frac{dN}{dD} = \int_{v_{min}}^{v_{max}} dV \int_{\theta_{min}}^{\theta_{max}} d\theta \left(\frac{dN}{dD_p}\frac{dD_p}{dD}\right) f(V) f(\theta) \qquad (3)$$

where $\qquad \dfrac{dN}{dD_p}$

is the size frequency distribution of projectiles (Ivanov 2001). This equation allows us to construct a model impact crater SFD. For asteroids and meteorites, data are often fitted for convenience by power law SFD, i.e., the differential distribution in the form

$$\frac{dN}{dD} \sim D^{-k} \qquad (4)$$

where k may vary from 2.95 up to 3.5 (Ivanov 2001; Hartmann 1969) in the size range we primarily consider here.

An independent treatment comes from crater statistics (Hartmann 1969; Neukum and Ivanov 1994; Ivanov et al. 2001; Neukum et al. 2001). The application of cratering scaling laws permits authors to estimate the size frequency distribution of projectiles from the measured SFD of lunar impact craters. Although this SFD can also be approximated in restricted size ranges by power law segments, Neukum has developed a single polynomial fit that fits the SFD over a wider size range and is supported by data on several planetary bodies. The papers referenced above suggest that craters on the moon and Mars were created by essentially the same family of projectiles.

We combine the above considerations with calculations on atmospheric bolide passage to generate the SFD for the martian surface. Our estimates show that the angle of impact, distributed as f(θ) ~sin(2θ), does not affect strongly the results except for extreme oblique impact. The effects of oblique impact are complicated, but these impacts have low probability, and we ignore them. On these grounds, we adopt the only a mean value of impact angle θ (θ ~45°) here and below.

To simplify the problem further, we use the velocity-average values of crater sizes < D > and omit the integration by velocity here. The simplified form of Equation 3 is as follows:

$$\frac{dN}{dD} = \left(\frac{dN}{dD_p}\frac{dD_p}{d < D >}\right) \qquad (5)$$

Let us now consider the atmosphere action on entering bodies and its action on the resulting crater population.

INFLUENCE OF ATMOSPHERIC DECELERATION AND ABLATION ON CRATERING

The first atmospheric effect we consider is the combination of deceleration and ablation. Vasavada et al. (1993) considered these effects martian atmospheres in the range of surface pressure 0.2–6 mbar and concluded that the production rates of cm-sized craters would be influenced by the atmosphere pressure variations. We will primarily consider bigger meteoroids and craters.

Meteoroids of different composition differ not only by strength but also by bulk densities, ablation energy, and heat transfer coefficients. We adopt the heat transfer coefficients found for Earth by Golub et al. (1996) for H chondrite (OC) and iron meteoroids, which are extrapolated here to martian atmosphere densities. Ablation increases importance as size decreases, and the possible variation of ablation coefficients by 2–3 times, due to varying atmosphere composition, does not change the crater distribution essentially, especially for large meteoroids (1 m and larger).

For carbonaceous chondrites (CC), we use coefficients for OCs, assuming that evaporation alone will not differ essentially for these substances. Observational data (see below) indicate a larger value of the ablation coefficient (which is equal to the ratio of heat transfer coefficient to ablation energy and drag coefficient) for CCs than for the OCs. We suppose that this difference may be caused by other physical mechanisms integrated into ablation (detachment of small grains, quasi-continuous fragmentation, etc). We will consider our ablation efficiency for C chondrites as a low boundary and estimate its influence on the results.

We consider different surface pressures (p_s), from 1 up to 1000 mbar. The fraction of initial body energy released on the planet surface is shown in Fig. 1a. The surface pressures are labeled on the curves. The denser the atmosphere, the smaller the energy a given meteoroid retains on reaching the ground. For example, a 1 m H chondrite meteoroid in the present atmosphere keeps about 90–95% of its initial energy, but in a 300 mbar atmosphere, it keeps only few percent. From deceleration and ablation effects alone, we can predict that appreciable energy loss (>30%) in the present atmosphere begins to occur only below meteoroid sizes of 0.3 m.

The dependence of crater diameter (D) on projectile size and atmosphere pressure is given in Fig. 1b for H chondrite meteoroids. For example, the present atmosphere begins to reduce the crater size (compared to an atmosphereless case) only for projectiles smaller than about 0.5 m, but if in a past atmosphere of 300 mbar, the effect sets in for projectiles closer to 10 m in size.

The resulting crater SFDs are given in Fig. 2. The main result is that the departures from the normal or "production function" SFD would not be easily detectable in crater counts unless atmospheric pressures exceeded 30 or even 100 mbar. The N_H log differential plots shows this depletion of small craters most vividly, and Fig. 2 also illustrates that the smoothing inherent in the cumulative plot tends to mask this effect. In the most dense atmosphere under consideration (1000 mbar), no impact craters are formed with D <26 m due to the low terminal velocity.

FRAGMENTATION THRESHOLD

Fragmentation of the bolides adds more drastic effects than mere deceleration and ablation. Different ways exist to estimate the conditions for meteoroid breakup in the atmosphere. Most of these approaches model the breakup
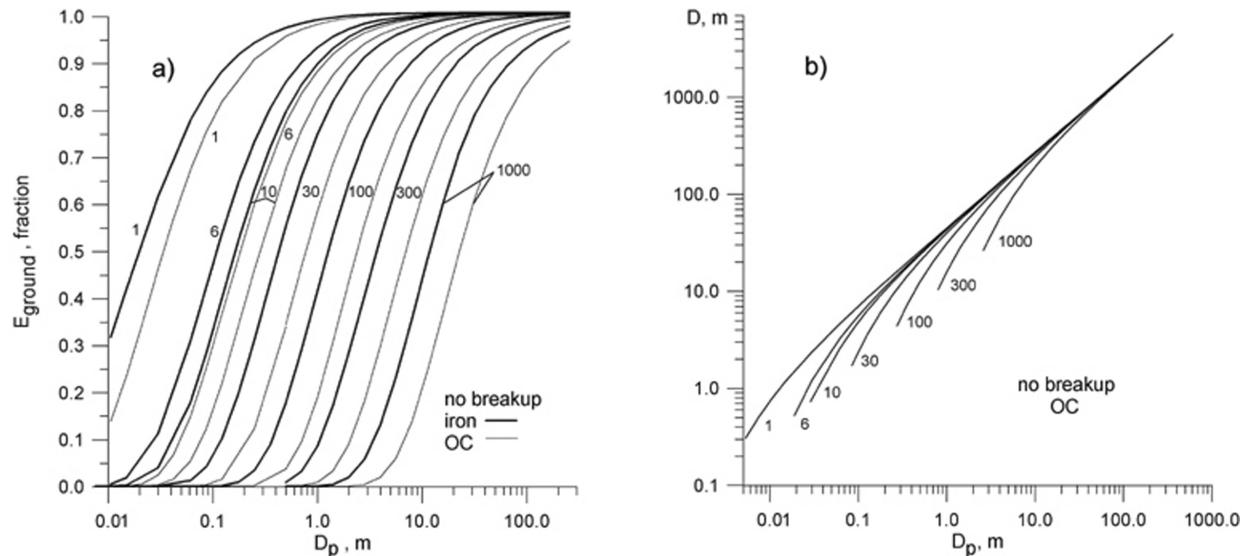

Fig. 1. a) Fraction of initial kinetic energy delivered to the ground (E_{ground}) as a function of projectile diameter (D_p) for different atmosphere pressures (labeled in mbar); b) diameter of crater (D) as a function of projectile diameter (D_p), assuming chondrite densities and no breakup. For small objects, drag and ablation result in low impact velocity and departure from the normal scaling laws.
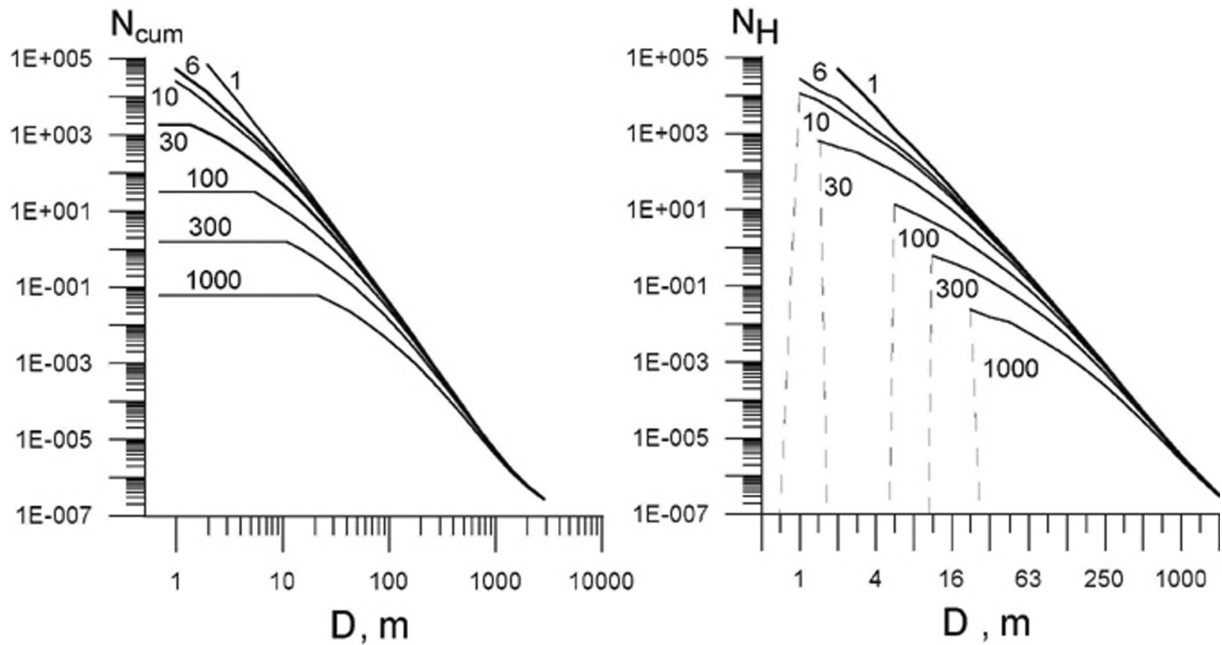
Fig. 2. Size-frequency distributions predicted on Mars for consideration of deceleration and ablation alone (not fragmentation) for different atmospheres (labeled in mbar). Two different styles of SFD plot are shown (see section on Crater Distribution): cumulative plot (cumulative craters/km^2 larger than D; left) and log-incremental plot (N_H = craters/km^2 in each $\sqrt{2}$ interval in D; right).

under aerodynamic loading, and different relations between meteoroid strength and breakup loading have been suggested (see Svetsov et al. [1995] for review).

Very limited data on meteoroid strengths are known. Empirical values of the apparent strength (σ_a) derived from bolide observations may be used along with strengths estimated from properties of meteorites. Some authors (for example, Hills and Goda [1993]) used the strength (σ_a) values derived from meteorites (σ_a ~100–500 bar for chondrites, σ_a ~2000 bar for irons), and estimated σ_a ~10 bar for comet debris with ice removed. However, note that in nature the effective strength of a large specimen tends to be lower than that of its smaller constituent volume units because of effects such as large-scale fractures. We use a strength scaling law (see below) to estimate the strength of big bodies based on the strengths of smaller samples. Meteorites demonstrate great scatter in the measured strength (Tsvetkov and Skripnik 1991; see Svetsov et al. [1995] for review). The average values of the tensile strength of small, less fractured chondrite samples (about 10 g in mass) may be estimated as 300–350 bar. The strength decreases as body size increases, according to statistical strength theory (Weibull 1951), consistent with the presumed history of parent body collisional fragmentation that produced the meteoroids themselves. The effective strength is estimated as

$$\sigma = \sigma_s(m_s/m)^\alpha \qquad (6)$$

where σ and m are the effective strength and mass of the larger body, σ_s and m_s are those of tested specimen, and α is a scale factor. This concept is partly empirical; in nature, it is generally found that larger rock masses are weaker than small ones due to the prevalence of fractures and inhomogeneities. Of course, occasionally, a large, strong, homogeneous rock mass may be found, but, generally, the concept is useful and argues against models where a giant meteoroid of ordinary chondrite composition is assumed necessarily to enter the atmosphere with an effective bulk strength equal to that of a hand specimen from a museum. There is no universally accepted value for the power exponent (α), but it may be estimated as about 0.1–0.5 for stony bodies (Svetsov et al. 1995). Given a spherical meteoroid's effective strength, the condition for breakup may be written as $0.365 \, \rho_a V^2 = \sigma_{ten}$, where ρ_a is atmospheric density (Tsvetkov and Skripnik 1991). This strength scaling law permits us to successfully describe the fragmentation of Sikhote Alin and Benešov meteoroids (Nemtchinov and Popova 1997; Borovička et al. 1998). Atmospheric fragmentation has been discussed by Foschini (2001). He discards the relation of $\rho_a V^2 = \sigma_a$ and regards models as inconsistent with observed high meteorite strengths. However, this relation is used for defining the apparent strength (σ_a), and we associate the low apparent strengths of initial breakup events with fractured states of the meteoroids, as discussed.

Observational data demonstrate that most bolides display fragmentation. According to Canadian bolide Network observations (Halliday et al. 1996), some fragmentation is common at all heights below 55 km.

Objects entering planetary atmospheres belong to different taxonomic types. According to several independent methods (Ceplecha et al. 1998), 5 main groupings of fireballs

can be distinguished among the larger Earth-entering meteoroids. The groupings differ in their ability to penetrate the atmosphere. Ceplecha et al. (1998) proposed fractions of bodies in the following groupings at the top of the atmosphere: irons = 3%, ordinary chondrites (Ceplecha group I) = 29%, carbonaceous chondrites (Ceplecha group II) = 33%, regular cometary material (Ceplecha group IIIA) = 26%, and weak cometary material (Ceplecha group IIIB) = 9%.

The apparent strength (σ_a) of 80 Prairie Network (henceforth, PN) bolides (relatively small bodies of 2–2000 kg) was estimated by Ceplecha et al. (1993) with the help of the gross-fragmentation (trajectory analysis) method. This study revealed that 38% of them were evidently fragmented during flight, while 36% were unclassified due to insufficient observations. Possibly, about 60% of PN bolides (smaller than 1 m in size) fragment during flight. All bodies marked as fragmented were disrupted under apparent loading <12 bar. Half of them were fragmented under loading <3.5 bar. Based on his analyses of density, ablation efficiency, and other data, Ceplecha et. al. classified these bodies as being of type I or II, i.e., ordinary or carbonaceous chondritic composition. Based on this work, we assume that some stony bodies may be disrupted at low pressure loading. Among PN bodies studied by Ceplecha et al. (1993), 4 meteoroids survived without fragmentation up to 15 bar, and 1 meteoroid survived as single body up to 50 bar. These represent stronger classes.

Several PN bolides were analyzed by radiative radius technique (Nemtchinov et al. 1994). This method allows us to estimate the moment of meteoroid breakup into a cloud of vapor and small fragments, which rapidly expands and creates flashes on the light curve. This type of fragmentation is more common at relatively low altitudes (40–20 km) under higher loading (Popova and Nemtchinov 1996; Borovička et al. 1998; Nemtchinov et al. 1997). The corresponding meteoroid strength is about 20–40 bar (Popova 1997).

Both methods of breakup analysis—gross fragmentation and radiative radius technique—were used in studying the large Benešov bolide (D_p ~1.2 m) and showed multistage disruption of this meteoroid. The radiative radius approach revealed two fragmentation points at altitudes of 40 and 24 km under loading of about 25–30 and 95 bar (Borovička et al. 1998). The presence of these breakup events was confirmed by direct observation of fragments during the flight. The dynamics of this meteoroid suggested a third, high-altitude breakup event under loading of 0.5–1 bar. Falls of meteoritic fragments were predicted for this fireball, but none were found, possibly due to the complex landscape of the fall site. Apparently, this may have been a pre-fractured object when it entered the atmosphere, beginning to breakup at around 1 bar, and then producing strong fragments that needed 25 to 95 bars for further breakup.

The next data set about behavior of large meteoroids in Earth's atmosphere is provided by the Satellite Network (SN). These data (Tagliaferri et al. 1994) were partially analyzed by Nemtchinov et al. (1997), and some results are shown in Table 1. Here, E_r is the energy of the radiation impulse, η is the luminous efficiency assumed for estimates of the initial kinetic energy (E_o) (Nemtchinov et al. 1997), M_0 is the initial mass, V_0 is the initial velocity, H_m is a characteristic altitude of the event, σ_a is the estimate of aerodynamic pressure leading to breakup. Projectile diameters (D_p) in Table 1 assume a meteoroid density of 3 g/cm^3 for simplicity. Velocities of 8 SN bolides are known due to infrared positional data or eyewitness data. For 5 events, the velocity was estimated during analysis by Nemtchinov et al. (1997). Characteristic fragmentation altitudes are usually associated with the height of maximum luminosity and are close to 30 km. Estimating that breakup occurs several km higher (Popova and Nemtchinov 2002), one may roughly estimate the breakup loading as $\rho_a V^2$. The value of breakup pressure causing formation of vapor and small fragments cloud was found to be about 20–50 bar with a large scatter.

Data on some other observed meteoroids for which data of breakup is known do not contradict to this estimate. For the Pribram meteorite the breakup loading was in the range 10–50 bar (Bronshten 1983). The Lost City meteoroid was disrupted in several stages (Ceplecha 1996) and the last breakup (H ~22 km) occurred under loading of about 25 bar (Ceplecha 1996; Popova 1997). The Peekskill meteoroid fragmented under loading of about 7 bar (Brown et al. 1994). The flash on light curve Innisfree bolide took place at about 35 km altitude under loading of about 18 bar (Halliday et al. 1981). All these bodies were ordinary chondrites. The breakup and bright flash, and correspondingly intense energy release, occurred under relatively high-pressure loading (higher than the 12 bar result found by Ceplecha et al. [1993]).

Meteoroid fragmentation is often a multistage process. More detailed study of some European Network (EN) and SN bolides (Marshall Islands, Greenland, Benešov, Moravka) suggests that the first fragmentation occurs at high altitudes (50–60 km) under pressure loading of a few bars, similar to that found by Ceplecha et al. (1993). If the meteoroid is large enough, first-stage fragments penetrate deeper into the atmosphere without essential deceleration and are fragmented once more. The number of second-stage fragments may be large enough that intense energy release results. Breakup pressures causing intense flashes on light curves of relatively big meteoroids appear to be about 20–50 bar, although we must remain aware of the possibility of breakup under either smaller or larger loading.

In spite of the low strength of carbonaceous chondrite meteorites, there are not yet any data demonstrating their different behavior during flight. The analysis done by Ceplecha et al. (1993) does not distinguish carbonaceous and ordinary chondrites by their strength. The difference is seen only in the ablation coefficient. However, useful data come from the large Tagish Lake bolide, which produced carbonaceous chondrite meteorite fragments (Hildebrand et

Table 1. Data of large meteorites in Earth's atmosphere.[a]

Event	Date	E_r (kt)	η (%)	E_o (kt)	M_o (ton)	D_p (m)	V_o (km/s)	H_m (km) Earth	$\sigma_a = \rho_a V^2$ (bar)	H_m (km) Mars
88106 (SN)[b]	15 Apr. 1988	1.70	11	8–9	25–45	2.5–3	48–50est	43	<9	20–21
90274 (SN)[b]	1 Oct. 1990	0.57	9.7	3–5	70–200	3.5–5	15–20est	30	10–30	0
91277 (SN)[b]	4 Oct. 1991	0.14	8.4	0.9	20	2.3	15–20est	33	12–30	4.5
94032 (SN)[b, c]	1 Feb. 1994	4.39	12.5	31	400	6.3	24[b]	34, 21	<8, >100	4.5, 0
94149 (SN)[b]	29 May 1994	0.090	8.0	0.6–2.5	2–140	1.1–4.5	<50est	34	<120	4.5
94307 (SN)[b]	3 Nov. 1994	0.56	9.7	3–5	70–200	3.5–5	15–20est	34[c]	<5–17	4.5
94350 (SN)[b]	16 Dec. 1994	0.0086	5.9	0.07–0.3	0.25–17	0.5–2.2	<40est	30	<200	0
94166 (SN)[b] (OC)	15 June 1994	0.0031	4.93	0.063	1–3[b]	0.9–1.2	13	36.2	6–10	8.5
El Paso (SN)[d]	9 Oct. 1997	0.045	7.5	0.6	8[e]	1.7	25	28–30[d]	54–100	0
Greenland (SN)[f]	9 Dec 1999	0.064	7.8	0.8	8[e] 36[g]	1.7[e]	29[f], 30.5[g]	46?, 28–25[f] 33–21[g]	<4, 130–230 100–400[g]	24?, 0 4.5–0
N. Zealand (SN)[h]	7 Jul 1999	–	–	–	?(1–3)	?(0.9–1.2)	–?(18)	28.8	?(50–70)	0
Yukon (SN)[h] (CC)[i, j]	18 Jan 2000	0.26	9.1	2.85	50–200[e]	3.2–5	15.8	37[i], 25[h]	<7, 20–40	10, 0
01113 (SN)[h]	23 Apr 2001	1.1	10.4	10.6	?(200–400)	5–6.3	–?(18)	28.5	?(<20)	0
Pacific Region[k]	14 Jan 1999	1.2	10.4	11.5	500[e]	6.8	15	35	<3	7
Benešov[l]	7 May 1991	0.01	6.1	0.16	2–4	1.1–1.4	21	37, 24	13–22, >120	10, 0
Peekskill[m] (OC)	9 Oct 1992	–	–	–	~10	1.9	14.7	41, below	>4	16
Mbala[n] (OC)	14 Aug 1992	–	–	–	0.4–1	0.6–0.9	13.5	25, below	60–70	0
Příbram[o] (OC)	7 Apr 1959	–	–	–	1–5	0.9–1.5	20.9	44–25	3–200	<21
Moravka(SN)[p, h] (OC)	6 May 2000	0.006	5.6	0.1	1–3	0.9–1.2	22	36, below	20–30	<8.5
Innisfree[q] (OC)	7 Feb. 1977	–	–	–	0.1–0.02	0.4–0.2	14	36, below	12–15	<10, 8.5
Sikhote-Alin[r] (I)	12 Feb. 1947	–	–	3.5–13	200–500	–	12–15	28–10	50–300	0

[a]CC = carbonaceous chondrite; OC = ordinary chondrite; I = iron.
[b]Nemtchinov et al. 1997.
[c]McCord et al. 1995.
[d]Hildebrand et al. 1999.
[e]Popova and Nemtchinov 2000.
[f]Ceplecha et al. 1999.
[g]Pedersen et al. 2001.
[h]USAF press release.
[i]Also known as Tagish Lake meteorite.
[j]Brown et al. 2001.
[k]Pack et al. 1999.
[l]Borovička et al. 1998.
[m]Brown et al. 1994.
[n]Jenniskens et al. 1994.
[o]Bronshten 1983; Ceplecha 1961.
[p]Borovička et al. 2001
[q]Halliday et al. 1981.
[r]Nemtchinov and Popova 1997.

al. 2000) and had D_p ~3–5 m (Popova and Nemtchinov 2000). It was catastrophically disrupted at an altitude above 25 km (apparent strength [σ_a] ~20–40 bar), according to SN data, or possibly an altitude of 37 km (σ_a ~3–10 bar), according to visual observations. These data imply strengths similar to the ordinary chondrite producing the St. Robert bolide, which had D_p ~1.2 m (Nemtchinov et al. 1997), $H_{fragm.}$ ~36 km (Brown et al. 1996), and σ_a ~11 bar. The strength also appears similar to that of the ordinary chondrite Moravka meteorite, which had D_p ~1 m, $H_{fragm.}$ ~50 to 30 km, and σ_a ~5 to 50 bar (Borovička et al. 2001).

Aerodynamic forces on these objects depend mainly on the atmosphere density and the shape, structure, and other properties of meteoroids, and, to a lesser extent, on the atmospheric chemical composition. Except at the smallest sizes, ablation is less important than fragmentation, which, in turn, depends mainly on the strength of the meteoroid. So, a cosmic body with given pre-atmospheric properties will decelerate and fragment in the martian atmosphere similarly to one in the Earth's atmosphere, roughly at levels where the density of the martian atmosphere is the same as that of terrestrial air. Thus, to check our theoretical simulations for present-day Mars, one may simply use observational data for the case of the Earth but with altitudes decreased by about 30 km. The data on the characteristic altitude deduced above the Earth, and also converted to Mars, are given in Table 1.

Before 1994, 14 meteoroids with sizes of the order of 1 m were observed photographically (Ceplecha 1994a, b). Five of them (about 30%) had end heights higher than 45–50 km altitude and revealed maximum luminosity at 90–60 km altitudes. Such high-altitude events generally correspond to the weakest bodies. One of these events, the Šumava bolide, was studied in detail (Borovička and Spurný 1996; Nemtchinov et al. 1999c). It was disrupted under loading of about 0.2–1 bar. These bodies were classified as Ceplecha's type III (i.e., cometary bodies) because of the apparent very low strengths, high ablation ability, and small bulk density. We note that Šumava-like meteoroids of 5000 kg or smaller would not reach the ground on present-day Mars. Nevertheless, larger meteoroids of similar structure and strength would penetrate to the surface and form craters. Additional modeling of such weak and probably volatile-rich bodies should be pursued.

To summarize this brief review of apparent strength of entering bodies: 1) cometary bodies are fragmented at the apparent strength of 0.1–1 bar; 2) carbonaceous chondrites and ordinary chondrites show a big scatter in apparent strength (Table 1), probably due, in part, to their pre-atmospheric collision history and condition of internal fractures. We assume 1, 5, and 25 bar as their apparent strengths, with 25 bar corresponding to the best solution for the maximum intensity of radiation of the bolide; 3) we consider iron meteoroids as either having very large strength (and no fragmentation) or (perhaps, if pre-fractured) being subject to fragmentation according to strength scaling laws (Equation 6, using α ~0.2 to 0.1 and referring to the Sikhote-Alin meteorites).

FRAGMENTATION EFFECTS IN THE LIQUID-LIKE ("PANCAKE") MODEL

Earth's observational data show that for the biggest bolides (20–2000 kg), two main types of fragmentation occur. The first is disruption into several large pieces moving separately, which may have their own separate histories of further fragmentation. In the second type, which we consider in this section, initially formed fragments move together deeper into the atmosphere and continue their breakup. If the time between fragmentations is smaller than the time for fragment separation, all the fragments move as a unit, and a swarm of fragments and vapor penetrates deeper, being deformed by aerodynamical loading, like a drop of liquid. This liquid-like or "pancake" model assumes that the meteoroid breaks up into a swarm of small bodies, which continues their flight as a single mass with increasing pancake-like cross-section. This approach was proposed and developed by Grigorjan (1979), Zahnle (1992), Chyba (1993), Chyba et al. (1993), and Hills and Goda (1993). Numerical simulations of the liquid-like fragmentation under aerodynamic loading show very complicated behavior due to the development of instabilities at the boundary (cf., Adushkin and Nemtchinov 1994; Svetsov et al. 1995; Nemtchinov et al. 1999b; and references therein). Here, we use a semi-analytical approach similar to that of the pioneering works mentioned above but with some modifications (Popova and Nemtchinov 1996; details given by Popova [1997]). The most intense flashes on the light curves of the largest terrestrial bolides, at the altitudes of 25–40 km, are well described by this model (Nemtchinov et al. 1997; Borovička et al. 1998). Slightly different equations exist for velocities of radius growth in literature (for review see Svetsov et al. [1995]). We assume that the velocity of radius increase (u) may be written as follows

$$u = kV\sqrt{\rho_a / \rho_m} \qquad (7)$$

where V is the velocity of the body, ρ_m is the density of the body, ρ_a is the atmosphere density, and k is constant. A heavily fragmented body is treated as a cloud of small fragments and vapor. The value of k is chosen as k ~0.3; this value proved to be the best in the modeling of the Benešov bolide light curve (Borovička et al. 1998) and also is close to the value found in numerical simulations of Crawford (1996) and Ivanov et al. (1997).

The maximum possible increase of radius of the pancake-like swarm of material is an open question. Some theoretical considerations suppose the radius may increase about 2–3 times (for example, Hills and Goda [1993]), whereas an

increase of radiative radius of 3–7 times and more is observed in bolide light curve analysis. We assume that the vapor cloud cannot increase more than five times and estimate that further increase of maximal allowed radius does not change the energy release essentially. The difference in the resulting crater diameters created by these uncertainties in the pancake model of the expanding meteoroid mass is estimated to be no more than 10–30%.

We treat fragmentation by assuming that breakup starts as soon as the aerodynamic loading equals the effective or apparent strength. We consider several values of apparent strength, 1, 5, and 25 bar, in the range obtained by observations. A comparison of energy fraction released on the planetary surface by non-fragmented and fragmented H chondrite meteoroids is given in Fig. 3a; a comparison of pancake models for two different values of strength (1 and 25 bar) is given in Fig. 3b. The fragmentation creates a threshold and shift to bigger meteoroid sizes in the energy release curves if the surface pressure exceeds 10 mbar. For dense atmospheres (p_s ~100–1000 mbar), the energy fraction released does not vary much with apparent strength. For less dense atmospheres (p_s ~1–30 mbar), including the present regime, the stronger bodies begin to reach the ground without breaking up. The difference between the present results and the final column of Table 1, which predicts breakup events for the martian atmosphere, is caused by the higher entry velocity of terrestrial bolides. For a given atmosphere and p_s, a critical crater diameter (D_{crit}) exists below which no high-velocity craters are formed. These critical crater diameters are given in Table 2. Under the present atmosphere, D_{crit} appears to be 0.5 to 4.5m for H chondrite bodies with strength 25 to 1 bar. The precise value of D_{crit} and the corresponding size of the projectile depend on the assumed criterion for crater formation and crater scaling law. Other scaling laws (see Melosh [1989] for review) and the adoption of another terminal velocity necessary for explosive crater formation could change results by about a factor of 2.

As the atmosphere density increases, the D_{crit} values for different strength H chondrite bodies are close to each other, and precise values of meteoroid strengths become insignificant in these cases.

In the Earth-like case of p_s = 1000 mbar, we find that fragmentation (coupled with the pancake model assumption) causes the disappearance of hypervelocity impact craters smaller than D ≅ 200 m, similar to the value of D ≤100 to 300 m that is seen on Earth itself. This cutoff drops to 32 m for p_s = 100 mbar; but, in this case, sub-meter-sized bodies hit the ground before fragmenting pressure is achieved and hold enough energy to form 4–8 m craters. Thus, from the cratering record alone, distinguishing the 100 mbar case from the present-day case at MGS/MOC resolution would be difficult, but cratering under p_s >300 mbar atmosphere would show a dramatic paucity of craters D = 80 m, compared to the present.

Corresponding crater SFDs are given in Fig. 4 and dramatically show the loss of small stony meteorite-caused craters for atmospheres in the pressure range of p_s >30–100 mbar and even p_s = 10 mbar for very weak objects. We use a liquid-like model of fragmentation with the strength scaling law Equation 6, and corresponding columns are included into Tables 2 and 3 as α = 0.25 and 0.5. The results found with this scaling law are close to that obtained with constant apparent strength. The specimen mass and strength are adopted to be 10 g and σ_s = 330 bar for H chondrites. The value α ~0.25 appears permissible for meteoroids similar to the SN objects (Popova and Nemtchinov 2002).
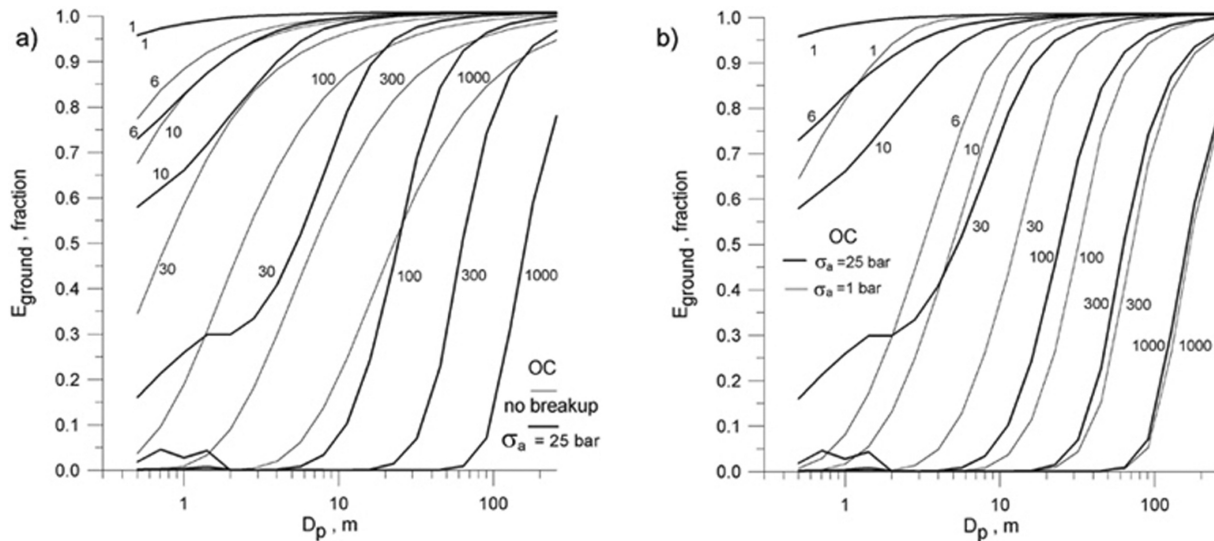

Fig. 3. The fraction of initial kinetic energy delivered to the ground as a function of projectile diameter, showing an H chondrite: a) first assumed to be affected only by drag and ablation (no fragmentation) and secondly with pancake model of fragmentation; b) different assumed apparent strengths.

Table 2. The boundary size of impact craters.

p_s mbar	H chondrite no breakup	H chondrite $\sigma_a = 25$ bar	H chondrite $\sigma_a = 5$ bar	H chondrite $\sigma_a = 1$ bar	H chondrite $\alpha = 0.25$	H chondrite $\alpha = 0.5$	Carbonaceous chondrite $\sigma_a = 25$ bar	Carbonaceous chondrite $\sigma_a = 5$ bar	Carbonaceous chondrite $\sigma_a = 1$ bar	Comet $\sigma_a = 1$ bar	Iron no breakup	Iron $\alpha = 0.2$
1	0.1	0.1	0.1	0.1	0.1	0.1	0.16	0.16	0.16	0.22	0.09	0.09
6	0.5	0.5	0.5	0.5, 4.5	0.5	10.5	0.7	0.7	6	8	0.3	0.3
10	0.7	0.7	0.7	6.6	0.7	0.7	1	1	8.6	11.7	0.5	0.5
30	1.7	1.7	14.4	15.6	1.7	1.7, 16	2.3	18.8	20.3	27.5	1.3	1.3
100	4.4	4.2, 32.3	37.8	38.8	4.4, 36	39	5.5, 41	48.4	49.9	66	3.2	3.2
300	10.4	82	86	87	86	88	104	109	110	143	7.5	7.5, 55
1000	26.4	201	205	207	206	207	246	252	254	312	19	153

Table 3. The size of projective forming boundary crater size given in Table 1.

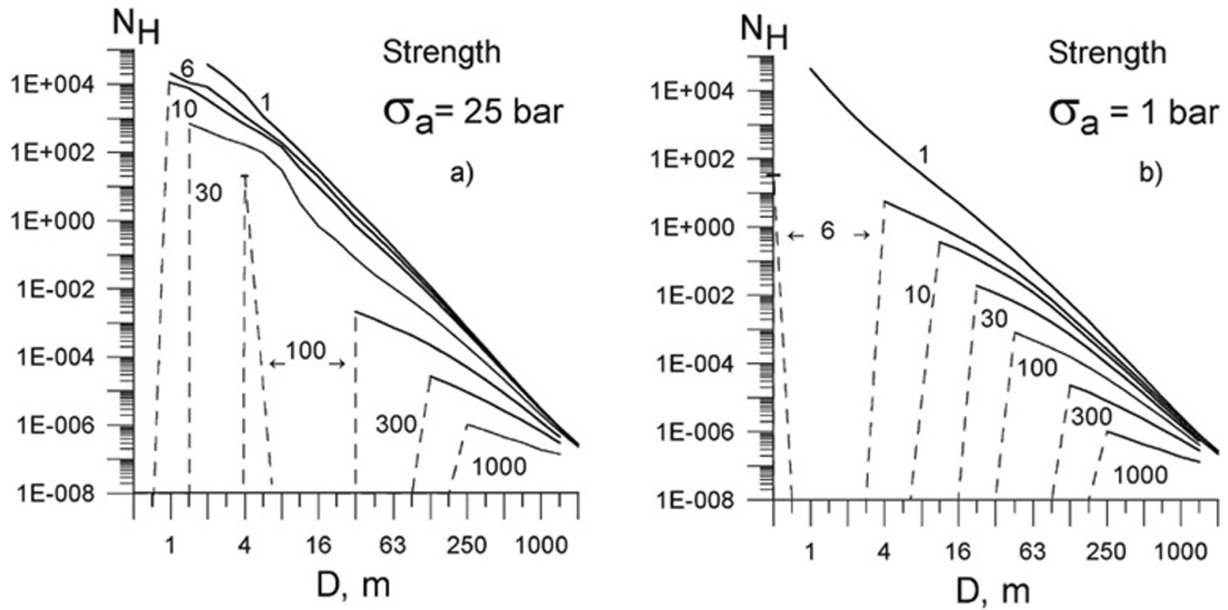| p_s mbar	H chondrite no breakup	H chondrite $\sigma_a = 25$ bar	H chondrite $\sigma_a = 5$ bar	H chondrite $\sigma_a = 1$ bar	H chondrite $\alpha = 0.25$	H chondrite $\alpha = 0.5$	Carbonaceous chondrite $\sigma_a = 25$ bar	Carbonaceous chondrite $\sigma_a = 5$ bar	Carbonaceous chondrite $\sigma_a = 1$ bar	Comet $\sigma_a = 1$ bar	Iron no breakup	Iron $\alpha = 0.2$
1	0.003	0.003	0.003	0.003	0.003	0.003	0.006	0.006	0.006	0.013	0.0015	0.0015
6	0.02	0.02	0.02	0.02, 0.5	0.02	0.02	0.035	0.035	0.9	1.7	0.01	0.01
10	0.03	0.03	0.03	0.75	0.03	0.03	0.05	0.05	1.4	2.8	0.015	0.015
30	0.08	0.08	1.9	2.2	0.08	0.08, 2.2	0.16	3.6	4	8	0.045	0.045
100	0.3	0.3, 5.4	6.5	6.7	0.3, 6.2	6.8	0.6, 9.5	11.6	12	24	0.14	0.14
300	0.8	17.4	18.4	18.7	18.4	18.8	30.5	32.6	33	62	0.4	0.4, 7.8
1000	2.6	54.7	56	56.5	56.4	56.8	93	95.6	95	168	1.3	28.4

Fig. 4. Crater SFDs for pancake-like fragmentation model applied to H chondrites, showing losses of small craters for different atmospheres. N_H gives the number of craters of diameter (D) (meters) in each $\sqrt{2}$-incremental log D bin (see Hartmann [1999] for further description of this type of plot). The curves represent different atmospheric pressures in millibars, as labeled. The top (1 mbar) curve corresponds approximately to the absence of atmospheric effects.

We must consider the smallest crater sizes expected from different classes of meteoroids to interpret not only data from future missions but also effects of impact gardening by the smallest impactors. Minimum sizes of projectiles striking the surface at >500 m/s are given in Table 3. For these small meteoroid sizes, ablation plays an essential role and we have used an ablation model. Vasavada et al. (1993) considered ablation and found that, for the current atmosphere, all meteoroids in the range of D_p ~0.4 to 20 cm are completely ablated. As a result, they predicted the smallest crater size to be about 3 m, but we believe that the ablation efficiency in that work is overestimated because of terrestrial experience.

Terrestrial data show that a fraction of cm-sized bodies (Bolide Network bodies) penetrates below 30 km altitude on the earth and would hit the martian surface. For example, according to Halliday et al. (1996), there were 46 probable meteorite drop objects among 754 fireballs with terminal mass >0.1 kg (and initial mass about 0.3–1300 kg [mainly 1–5 kg]).

For martian conditions, even more meteoroids should survive down to the ground due to lower average entry velocity. The lower the entry velocity, the lower the efficiency of ablation (Golub' et al. 1996). Theoretical consideration demonstrated that the ablation coefficient depends on size, height, velocity, and meteoroid composition (Golub' et al. 1996). For cm-sized bodies, this result is an ablation coefficient of about 0.003–0.023 s^2/km^2, depending on altitude and velocity (Borovička et al. 1998). The stony Moravka bolide ablation coefficient is also as low as 0.003 s^2/km^2 (Borovička et al. 2001).

Observational data allow us to determine the ablation coefficient for much of the meteoroid trajectory (Ceplecha et al. 1999), but its velocity dependence is not known. According to Ceplecha et al. (1999), the ablation coefficient varies with composition by as much as a factor of 10, is maximal for cometary bodies (~0.1–0.2 s^2/km^2), and is minimal for ordinary chondrites (~0.014 s^2/km^2) on average. Hörz et al. (1999) favored a value at the higher end of this range, while we have used values near the lower end. We possibly underestimate the ablation efficiency, and our results concerning boundary meteoroid size given in Table 3 could be increased as much as 1.5–2 times.

We found that under current conditions, the boundary size of impact crater may be 0.3 m and is formed due to the impact of ~1 cm iron body. The uncertainty of the minimum crater diameter estimates may be about a factor of 2.

Tables 2 and 3 include meteoroids similar to carbonaceous chondrites with $\rho_m = 2$ g/cm^3, assuming apparent strengths of 25, 5, and 1 bar. Due to the bigger effect of deceleration, the boundary values of projectile and crater size are bigger than for H chondrite meteoroids. We also consider cometary bodies (with ρ_m ~1 g/cm^3) and apparent strength of 1 bar. All critical cometary cutoff diameters are shifted to bigger sizes for a given pressure. Note that our size estimates for C chondrites and comets should be considered as low boundary (see also the discussion in the section on Influence of Atmospheric Deceleration and Albation on Cratering).

We were interested in comparing the smallest predicted crater sizes with the MGS/MOC resolution limit for good

crater counts, around 11 m. The smallest values of D_{crit} and D_p correspond to nonfragmented iron bodies. We also predict formation of 30–50 cm impact craters under current atmospheric conditions due to the impact of 1–4 cm stony and iron bodies. This is comparable to the results of Hörz et al. (1999), whose ablation impact model also predicts smallest craters in the "sub-meter" range, formed from strong stones and irons a few cm in size. Figure 5 shows data from Table 2. Fragmentation has no influence on strong, small stony bodies in the current atmosphere. The minimum size of weak H chondrite impactors ($\sigma_a = 1$ bar) is about 50 cm, and the smallest impact crater in our model is about 4.5 m. For cometary bodies, our assumptions yield a meteoroid diameter of about 2 m, forming 8 or 9 m craters, just below the MGS/MOC resolution limit.

For a denser atmosphere of $p_s = 100$ mbar, the smallest impact crater size is about 3 m for an iron meteoroid. Undisrupted stony bodies also may form craters of about 4–5 m in size. For still denser atmospheres, the minimum impactor body size increases to about 5–10 m for all weak or fragmented stony bodies with a minimum crater size of 30–50 m. Thus, during (Noachian) periods when the atmosphere exceeded a few hundred millibars, there should have been no craters below 30–50 m in size formed by stony and cometary bodies and only a few decameter-sized craters formed by the relatively infrequent irons. The crater deficiency would be difficult to detect, however, due to the populations of subsequent small craters formed under the later, thinner atmospheric conditions.

PROGRESSIVE FRAGMENTATION MODEL AND CONSEQUENCES ON CRATERING

Modeling the actual disruption of the body in the atmosphere is the biggest problem for the liquid-like model. This model assumes movement as a collective swarm and does not take into account that some parts of the body may be stronger than other parts, surviving to the ground and producing meteorites. Thus, we introduce a progressive fragmentation model, which assumes that separate fragments form at the moment of breakup and spread laterally. These fragments continue their flight separately from each other and can be disrupted during further flight. Both types of fragmentation—progressive fragmentation and "liquid-like" fragmentation—are observed among terrestrial bolides.

Progressive fragmentation has been considered in a number of works since 1956 (Levin 1956, 1961; Fadeenko 1967; Baldwin and Sheaffer 1971). In most cases, the fragmentation into a number of fragments is described without taking into account the lateral spreading of fragments. However, Passey and Melosh (1980) considered the aerodynamical interaction of fragments due to the compression of gas between them in the bow shock waves and the force that bow shocks exert on each other, and they
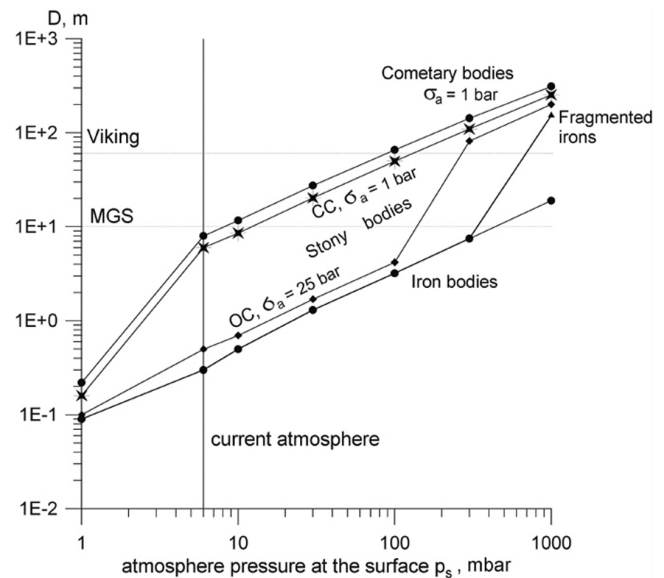

Fig. 5. Summary diagram showing the expected sizes of the smallest explosion craters (D, meters) on Mars for different atmospheres, for each meteorite class. For the present atmosphere, the smallest craters are around 5–10 m for weak meteorites and a few centimeters for irons and strong stones.

suggested that the velocity (u) of the fragment repulsion can be described by Equation 7. They analyzed terrestrial crater fields and found the constant (k) to be 0.14 to 1.22.

Artemieva and Shuvalov (1996, 2001) modeled the interaction of two fragments by direct 3D gas-dynamical simulations and found that the coefficient (k) in Equation 7 is about 0.45 for two equal cubic fragments. If the fragments are not equal, the lateral velocity of the smaller fragment will be higher. In the case of a meteoroid initially disrupted into 13 or 27 cubic fragments with cracks between them (Artemieva and Shuvalov 2001), the lateral velocity that defines the debris cloud radius can be written in the form of Equation 7, but the coefficient (k) is higher: ~1. In their latest paper (Artemieva and Shuvalov 2001), the evaporation of fragments was taken into account but it did not substantially change the mechanical forces and coefficient (k). Note that their result was obtained only for ordinary chondrites. Volatile-rich meteoroids need to be studied.

Comparison of lateral fragment velocities with Earth bolide and meteorite data shows that the value of (k) should be at least ~1 or even more (Borovička et al. 1998). We start with k ~1 in our estimates and increase it in certain cases, depending on relative momentum among the fragments. We successfully used these lateral velocity estimates to describe the Sikhote-Alin crater field and Benešov bolide fragments dynamics (Nemtchinov and Popova 1997; Borovička et al. 1998).

The progressive fragmentation model can be used if the number of fragments is not too large and if the fragments are well separated. If the time of fragment interaction is greater

than the time interval between two fragmentations, the fragments demonstrate collective behavior, as in the liquid-like model (see Svetsov et al. [1995] for review). In an ideal case, fragments of a body larger than a certain size would not have time to separate and would follow the liquid-like model, making one crater, while below that size, the fragments would separate, and the smaller bolide's behavior would follow the progressive fragmentation model, making several craters. We find that for chondritic bodies with the exponent $\alpha = 0.25$, the progressive fragmentation model may be used with a size of D_p $\sim \leq 10$ m in the current martian atmosphere. The 10-m projectile would form a crater of $D \sim 90$–230 m in the case of 6–100 mbar atmospheres, according to the pancake model. The range of predicted transitional crater sizes, where single craters may start to give way to strewn fields of craters, is sensitive to the adopted model of breakup. We cannot yet determine what model is better around this size, so we will note the differences in resulting pictures under these two models. Note also that the lateral velocities of the fragments are important in determining the dimensions of strewn fields formed in the breakups. Separated fragments may even form single craters in the case of small dispersion of the fragments.

Given the atmospheric density and strength law, the transitional crater size, i.e., the maximum crater size produced by the fragments in the progressive fragmentation model, is constrained to some degree. The value is determined by the maximal fragment size surviving in a given atmosphere, which does not depend on initial meteoroid mass, according to our law of effective strength versus size. In dense atmospheres ($p_s \sim 300$–1000 mbar), small separated fragments are decelerated much more effectively than a massive single body, and because of atmospheric drag, no hypervelocity impact craters are formed by the fragments, throughout the range of model validity. Thus, in dense atmospheres above 300 mbar, fragmentation processes should cause a dramatic decrease in crater number (N) in SFD below crater sizes of about 200–300 m, similar to the paucity of <300 m explosion craters on Earth. The predictions of both fragmentation models coincide in that sense.

CRATER SFD CAUSED BY TOTAL METEOROID POPULATION

At this point, we are facing the problem of how the meteoroid breakup and production of fragments affects the crater SFD observed on the ground. While we lose the meteoroid itself, we must take into account the craters added by the pieces of the fragmenting meteoroid. What are the realistic sizes of the fragments? If an ordinary terrestrial rock is shattered with low energy density, the largest pieces may be half the size of the original. But, as energy density increases, the largest surviving pieces are smaller (Hartmann 1969). Atmospheric breakup is a high energy density event, in this sense, and we note in Table 1 that several meter-sized

chondrites have produced decimeter-sized, low-impact-velocity specimens, while a number of larger objects, like the Tunguska and Greenland bolides, apparently produced no recoverable specimens that large. Possibly, they enter the atmosphere with pre-existing fracture planes or granular structure that cause them to fragment into very small constituent pieces. Very small fragments do not make explosion craters at all because they fall to the ground at low terminal velocities affected by drag or get blown away in the atmosphere altogether. To treat the craters produced by the fragments from breakups, we need to know the size of the largest fragment, the size distribution of the fragments, and the impact velocities of those fragments. This requires improved modeling in future work, but we attempt a preliminary treatment here.

As before, we assume the following meteoroid fractions: 3% irons, 29% ordinary chondrites, 33% carbonaceous chondrites, and 35% cometary. First, we will not include fragmentation. The total SFDs of craters from the undisrupted meteoroids are given in Fig. 6a. Note that in atmospheres denser than 100–300 mbar, the deceleration and ablation begin to cause deviations of the martian SFD from the lunar SFD at crater diameters smaller than 100–500 m. This is similar to our conclusion from Fig. 2 but is now much more general because we have found that all classes, not just chondrites, produce craters.

We start this discussion with the liquid-like (pancake) model, which calls for all fragments to hit the ground together in one area and make a single crater.

To estimate the fragmentation influence over a range of strengths, we consider the following meteoroid strengths parameters. For irons, we use the specimen strength of $\sigma_s =$ 440 bar for a 1 kg specimen size and scaling of $\alpha = 0.2$ (see discussion in the Fragmentation Threshold section). For chondrites, we use the apparent strength = 25 bar (that is similar to specimen strength of $\sigma_s = 330$ bar for a 10 g specimen size with $\alpha = 0.25$; carbonaceous chondrites $\sigma_a = 5$ bar; cometary bodies $\sigma_a = 1$ bar). We use the pancake model and find evident fragmentation, especially for denser atmospheres (Fig. 6b).

The effects of fragmentation on the SFD are seen even for the present atmosphere and are more pronounced in denser ones ($p_s > 30$ mbar). Under the present atmosphere, the main cratering contribution ($D \sim 1$–1000 m) comes from ordinary chondrites, but as the atmosphere pressure increases ($p_s > 30$ mbar), stony bodies are increasingly lost by breakup. At 100 mb, irons make the main contribution to cratering in the $D \sim 4$–200 m range. Although stony bodies are still producing craters down to 30–40 m in size, their contribution to total SFD in $D \sim 30$–200 m is smaller than that of iron meteoroids. Even above the crater size resolved by MGS/MOC ($D \sim 10$ m), the log incremental plot (N_H) shows a dramatic cutoff of small craters as p_s increases from 100 to 300 mbar and above (Figs. 5 and 6b).
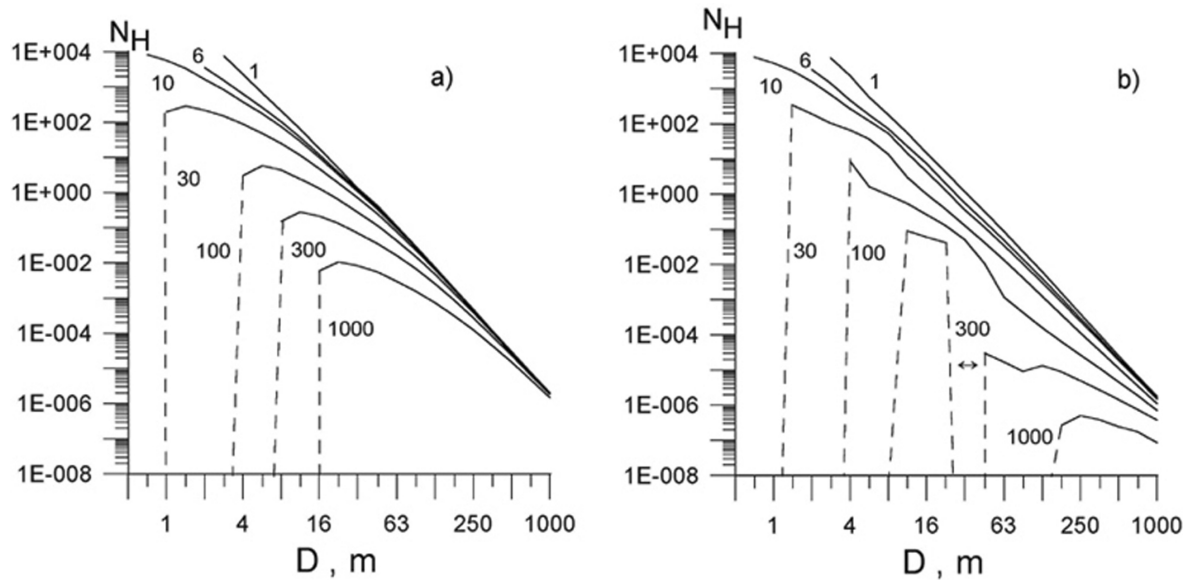
Fig. 6. Crater SFD predicated by adding all classes of meteorites, from weak bodies to irons: a) in an absence of fragmentation; b) including fragmentation even for irons. Plotted as in Fig. 4.

We also investigated the case where lower strengths are assumed for most meteoroids (irons—the same as in the previous case; OC σ_a = 5 bar; CC σ_a = 1 bar; comets σ_a = 0.1 bar). These weak bodies are effectively fragmented by present atmosphere, and craters 3–100 m in size are formed mainly by irons. At 100 mbar, the SFD is close to the case of the strong bodies, considered above, except for meter-sized craters. Small stony meteoroids are able to form these craters if σ_a = 25 bar. At p_s >100 mbar, the cratering efficiency is only slightly dependent on the precise values of stony/cometary meteoroid strengths in the considered strength range.

What are the main effects of fragmentation on the final SFD of craters observed on Mars? We have described how the liquid-like model may underestimate the fragmentation and cratering influence for decameter bodies. The turndown boundary on SFD will be more dramatic, i.e., shifted to bigger crater sizes, if one takes into account progressive fragmentation. In the present atmosphere, the fragments of the broken weak meteoroids would make clusters of high-velocity craters at very small crater sizes (probably meter scale or smaller), adding to the crater population that would be predicted from the unaltered production function SFD. In hypothetical denser past atmospheres, still bigger meteoroids breakup. One might expect bigger fragment-caused craters, but the fragments would be subject to greater pressure loading and would break into smaller pieces, as implied by our adopted law of strength versus size. Moreover, they would face increased drag in the denser atmosphere and tend to hit the ground too slowly to make normal explosion craters. In the other direction, as we approach p_s = 0 mbar, eventually no fragmentation and no fragment-caused craters exist. Therefore, one can see that at some atmospheric pressure, and depending on meteoroid strength distribution, a maximum

effect of fragment-caused craters added to the SFD must exist, and these effects will probably be found among decimeter- or meter-scale craters below the present 11 m limit of MGS/MOC crater resolution.

How do we search for atmospheric cutoff effects and possible strewn fields of small craters? One important factor should be taken into account. Small craters are lost due to dust infill, dune deposits, etc. (Hartmann 1971; Hartmann and Neukum 2001), complicating any claims of detection of deficiencies due to loss of small bolides. These factors are probably least important for craters formed on the young hard-rock lava flow surfaces that have been detected on Mars (Hartmann and Berman 2000; Hartmann and Neukum 2001), and these surfaces would be ideal to conduct further tests of the atmospheric cutoff effects on small craters, from about 0.1 m to 10 m in size, during future missions.

DETECTING PAST ATMOSPHERIC VARIATIONS

These discussions raise intriguing potential for using the cratering record to reveal past variations in the atmospheric pressure of Mars. We have mentioned 3 main effects that could arise during past periods of high atmospheric density: 1) dense atmospheres deplete small craters (4 previous sections). For example, during any period when the atmosphere had periods with pressure over 300 mbar, no hypervelocity craters will exist smaller than about 80 m, except for the irons and strongest stones, which are a fairly small fraction of the total (Table 2 and Figs. 4 and 6b). However, it will not be easy to detect such variations from the cratering record because the subsequent (present) thin-atmosphere condition leads to an overlying population of small craters, which are very numerous because they lie in the

steep part of the SFD; 2) dense atmospheres produce more clusters of small craters from atmospheric events (Fragmentation Threshold section and the 2 sections before the current section). We expect the craters to be small, e.g., tens of meters in scale and spread over clusters up to about a km in scale, not unlike the terrestrial strewn-field case (see next section). This effect should be preserved in cratering records; and 3) dense atmospheres break up stones, leading to dominance of irons as creators of mid-sized, 10–100 m-scale craters (as on Earth), while the present martian atmosphere would allow dominance of stones as source of these craters (previous section). This effect should be observable but would require sophisticated ground based sampling.

The use of crater populations to study ancient atmospheres leads to several specific cases of interest.

Noachian Higher Pressure Periods

That the Noachian atmospheric pressure was greater, perhaps up to hundreds of mbar has been widely suggested. The crater cutoff we find at 300 mbar is D ~80–100 m as mentioned above, and even for 1 bar, it rises only to D = 200 m. A population of craters due to irons and strong stones might reach smaller sizes (D ~20 m). If such an atmosphere dwindled by the end of the Noachian or Hesperian periods (perhaps causing the end of those periods), then the loss of that atmosphere would have occurred by 2000 to 3500 Myr ago, according to the chronology of Hartmann and Neukum (2001). However, according to the modern crater production and gardening rates developed by Hartmann and Neukum (2001), Ivanov (2001), and Hartmann et al. (2001), craters in the size range of 40 m to 200 m reach saturation under modern conditions in as little as only about 200 Myr to as much as 3000 Myr, respectively. Therefore, detecting the turndown in the population of small craters created during a Noachian high-pressure period would be difficult.

However, recent observations of Mars increase the probability that some ancient surfaces of Mars have been buried by sedimentary layers and recently exhumed (Malin and Edgett 2000) and that these surfaces may preserve ancient crater populations (Greeley et. al. 2001; Hartmann et al. 2001, pp. 49–51). On such ancient, preserved surfaces, behavior of the original small-crater population might be difficult to confirm because of obliteration effects, but tell-tale clustering of craters due to dense-atmosphere fragmentation events might be observable from orbital imagery, and composition signatures of the impactors might be observable on the ground.

Recent Higher Pressure Periods

Plausibly, obliquity variations or volcanic outbursts might have increased martian surface pressures in more recent times. Malin et al. (2001) argue that the atmosphere has changed on very short timescales of less than 1 Myr. The recent pressures seem very likely to have risen above the 100 mbar levels widely postulated for early Mars. At pressures <100 mbar, the atmospheric meteoroid losses are primarily represented by crater losses in the (D) range of 10 to 40 m for the various stony meteorite types. This is near the cutoff in resolution for MGS/MOC images and would be hard to document in current imagery. Furthermore, these craters resaturate in only about 10 Myr to 200 Myr, respectively, according to the cratering rate data above, so the putative high pressure periods would have to have reached many tens of mbar, been fairly long-lived, and recently ended to leave a detectable signature in loss of very small craters. According to Fig. 6b, recent transient higher-pressure episodes at <100 mbar would also be hard to detect through crater clusters due to fragmentation events.

Low Pressure Periods

Under the current 6 mbar pressure, hypervelocity craters, even produced by irons, would be formed at sizes down to D ~0.3 m (Fig. 5). Hörz et al. (1999) found a similar result and asserted the detection of spall craters 0.25 m across on rocks in Pathfinder photos. As noted by Hörz et al. (1999), rock surfaces offer much better preservation of such small craters than loose or lightly cemented martian soils. Plausibly, obliquity variations might have created periods of lower atmospheric pressure than the current 6 mbar. During these periods, rocks on the surface might be hit by even smaller meteoroids that would otherwise be blocked by the 6 mbar atmosphere. Through future rover missions or human landings, spall marks and "zap pits" of this sort might be sought in surface rocks to confirm atmospheric variations. This effect might also be detected by comparing the highest elevation sites with low elevation sites.

GARDENING EFFECTS

If the long term average of the atmospheric pressure during Amazonian times has been <100 mbar, our results indicate that the cratering by abundant small bodies guarantees a certain degree of gardening effects, although, the lack of micrometeorite "sandblasting" means that the regolith so produced would be coarser than on the moon. Hartmann et al. (2001) discussed such gardening in more detail and showed that the geometry of crater coverage and saturation require martian regolith production regardless of the absolute ages of the surface units. martian winds would mobilize the finest debris, and the removal of fines from coarse regolith may be a factor in producing the boulder-strewn landscapes seen by the first 3 landers.

As for more ancient times, we have shown that the hypothetical denser atmosphere would have resulted in the loss of still more small craters. Nonetheless, saturation would

again guarantee gardening effects. Direct crater counts in the existing uplands show that saturation was at least approached at crater sizes around 45–64 km. Probably, smaller craters also reached saturation but have been lost subsequently due to erosion effects (Hartmann et al. 2001). Thus, megaregolith should have been produced on Noachian Mars down to depths of km scale. Our results in this paper suggest that, under a Noachian atmosphere of a few hundred mbar, impact cratering would not occur below decameter scale, and this would ensure that the early martian megaregolith would be substantially coarser than the lunar example. The coarse early megaregolith would probably have served as a very efficient sink for early martian water, which may exist today as large masses of ground ice mixed into the coarse, upland fragmental layer.

MARTIAN CRATER CLUSTERS

During examination of Viking pictures, numerous, seemingly isolated clusters of 500 m scale craters, in patches 5 to 20 km across, were noted on Mars (Hartmann and Engel 1994). An example is shown in Fig. 7. Hartmann and Engel suggested that these might represent breakups of unusually weak, cometary bodies in the high atmosphere. Such a hypothesis would require lateral spreading of fragments at speeds on the order of 300 m/s to attain the observed spreading during atmosphere passage, as judged by u = (cluster radius/atmosphere flight time). Such lateral spreading speeds were indeed observed among small, kg-scale fragments of the Benešov (Borovička et al. 1998) and Moravka (Borovička et al. 2001) bolides. However, our current investigations of the lateral spreading of fragments do not allow such high velocities among the larger, crater-forming fragments of the bolide disruptions we are considering for Mars. In the current model, the lateral velocity depends on the altitude and entry velocity (Equation 7). For an entry speed of 20 km/s, the lateral velocity is about 27 m/s for breakup of a stronger body at 10 km altitude. These figures do not allow enough time for the creation of such large clusters as are observed on Mars. We are currently investigating various effects that might produce the observed clusters, including: 1) explosive gas production that might drive apart weak, ice-rich fragments making up a comet; 2) disruption of cometary bodies by tidal forces, impacts, or other processes at some distance from Mars, before entry; 3) ejection from martian craters of secondary blocks, which disperse during flight upward through the atmosphere and fall back at random locations, making clusters; and 4) dislodging of fragmenting blocks of secondary ejecta from impacts on Phobos or Deimos.

Our ongoing work with the progressive fragmentation model applied to the present atmosphere predicts some fragmentation among modest-sized weak bodies, which should produce clusters of small impact craters tens of meters
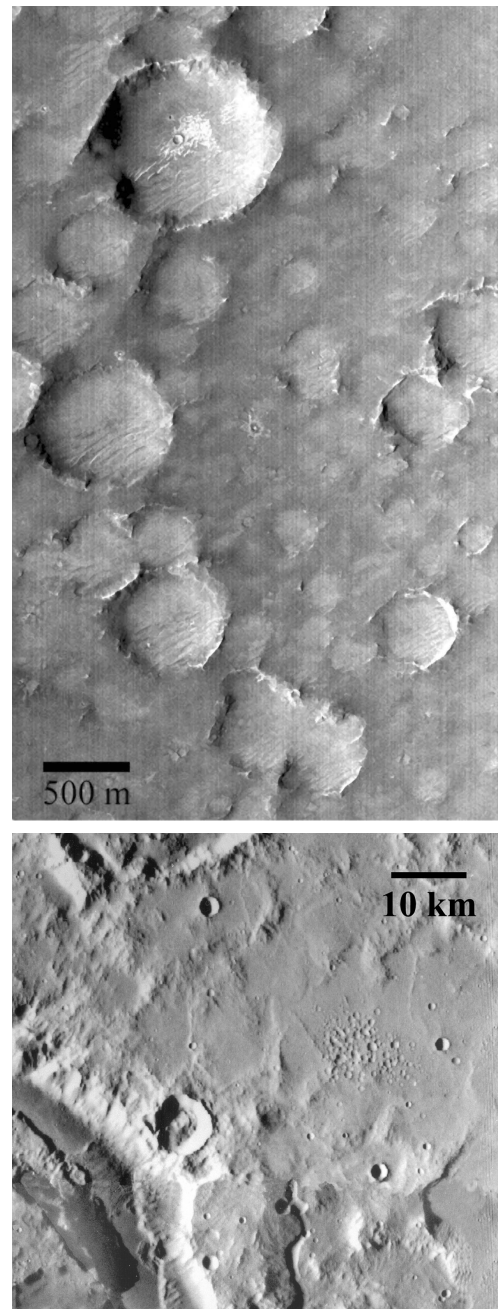

Fig. 7. a) East portion of cluster of overlapping 700 m-scale in MGS image 12–014325, at latititue –20°S, longitude 182°W; b) Viking context mosaic showing surrounding area, next to Ma'adim Vallis. The cluster seems isolated, without an obvious recent parent crater that could act as a source of secondaries. This type of cluster appears to have too great a width to be accounted for by our modes of fragmentation of primary meteoroids but might involve isolated blocks of secondary ejecta lofted at near-escape velocity.

in size and scattered over regions of the order of 100 m in diameter. A possible example is shown in Fig. 8.

We intend to report on the phenomena of clusters of large craters, as well as clusters of small craters, in more detail in our planned second paper.
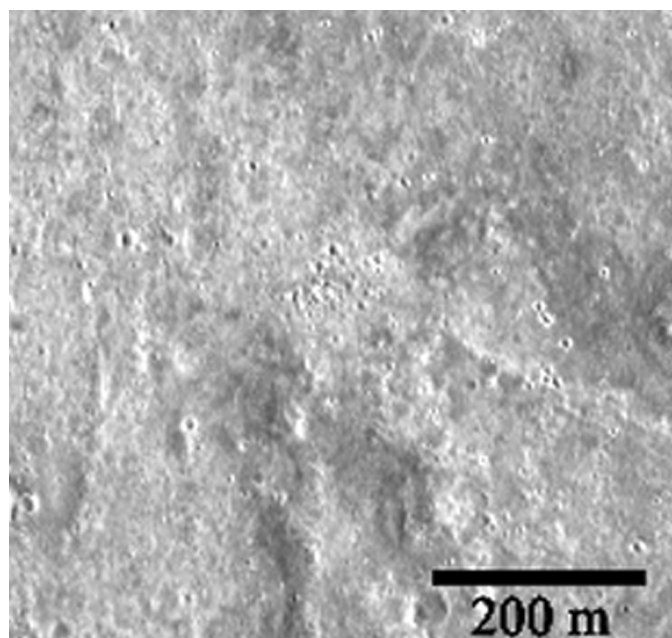
Fig. 8. This MGS/MOC image shows what appears to be a cluster of 10 m-scale craters spread over a few hundred meters. Unlike Fig. 7, this appears to match our predicated product of meteoroid fragmentation in the current atmosphere.

CONCLUSIONS

The smallest craters expected under current atmospheric conditions on Mars have diameters the order of 0.3 m due to iron meteorites that survived atmospheric passage. They might best be detected on martian rocks, as discussed by Hörz et al. (1999). The smallest martian craters due to stony meteoroids range from 0.5 to 6 m in diameter, depending on the strength of the meteoroids, and the smallest craters due to hypothetical weak icy or icy/carbonaceous cometary meteoroids would be about 8 m across.

The proposed presence of a complete production function size distribution of craters down to meter or sub-meter scale guarantees some impact gardening effects on the evolution of older surfaces. This may also be a factor in generating martian dust and obliterating distinctive ancient deposits such as lakebed evaporates.

Fragmentation influences the crater formation process on Mars, but primarily in hypothetical denser past atmospheres. In the present atmosphere, only the weakest bodies, with strength of ~1 bar, would fragment. As summarized in the previous section, and discussed in more detail in our forthcoming paper on crater clusters, the progressive fragmentation model predicts clusters of small craters with a diameter (D) of order 1–10 m, spread over a few hundred meters. Therefore, small crater clusters formed by our predicted contemporary breakup of ordinary stones and irons under ~30 to ~300 mb may be hard to distinguish from the small clusters formed by weak stones in the present atmosphere. Craters much smaller than 0.3 m (such as "zap pits" in rocks) would be diagnostic of earlier periods with lower atmospheric pressure, perhaps caused by obliquity variations.

As can be understood from this paper, reality is more complex than the existing models. To improve the modeling and reach a better understanding of Mars, new work is needed on subjects such as: 1) improved fragmentation modeling to reconcile the liquid-like and progressive fragmentation models; 2) a better understanding of the ablation parameter, especially for volatile-rich bodies; 3) a better modeling of the lateral separation of fragments, especially among volatile-rich bodies where gas production may affect the interaction of shock waves and lateral forces; 4) a better modeling of the fate of the fragments produced by disruptions, taking into account their size distributions, terminal velocities, and resulting craters; and 5) higher resolution imagery of selected surfaces (including ground imagery of smooth rock surfaces) to search for crater depletion and/or "zap pit" effects.

REFERENCES

Adushkin V. V. and Nemtchinov I. V. 1994. Consequences of impacts of cosmic bodies on the surface of the Earth. In *Hazards due to comets and asteroids,* edited by Gehrels T. Tucson: University of Arizona Press. pp. 721–778.

Artemieva N. A. and Shuvalov V. V. 1996. Interaction of shock waves during the passage of a disrupted meteoroid through the atmosphere. *Shock Waves* 5:359–367.

Artemieva N. A. and Shuvalov V. V. 2001. Motion of a fragmented meteoroid through the planetary atmosphere. *Journal of Geophysical Research* 106:3297–3310.

Baldwin B. S. and Sheaffer Y. 1971. Ablation and breakup of large meteoroids during atmospheric entry. *Journal of Geophysical Research* 76:4653–4668.

Bland P. A. and Smith T. B. 2000. Meteorite accumulations on Mars. *Icarus* 144:21–26.

Borovička J. and Spurný P. 1996. Radiation study of two very bright terrestrial bolides and an application to the Comet S-L 9 collision with Jupiter. *Icarus* 121:484–510.

Borovička J., Popova O. P., Nemtchinov I. V., Spurný P., and Ceplecha Z. 1998. Bolides produced by impacts of large meteoroids into the Earth's atmosphere: Comparison of theory with observations. I. Benešov bolide dynamics and fragmentation. *Astronomy and Astrophysics* 334:713–728.

Borovička J., Spurný P., and Ceplecha Z. 2001. The Morávka meteorite fall: Fireball trajectory orbit and fragmentation from video records. *Meteoritics & Planetary Science* 36:A25.

Bronshten V. A. 1983. *Physics of meteoric phenomena.* Dordrecht: Reidel. 356 p.

Brown P., Revelle D. O., and Hildebrand A. 2001. The Tagish Lake meteorite fall: Interpretation of physical and orbital data. Proceedings, Meteoroids 2001 Conference. pp. 497–505.

Brown P., Ceplecha Z., Hawkes R. L., Wetherill G., Beech M., and Mossman K. 1994. The orbit and atmospheric trajectory of the Peekskill meteorite from video records. *Nature* 367:624–626.

Brown P., Hildebrand A. R., Green D. W. E., Page D., Jacobs C., ReVelle D., Tagliaferri E., Wacker J., and Wetmiller B. 1996. The fall of the St. Robert meteorite. *Meteoritics & Planetary Science* 31:502–517.

Ceplecha Z. 1994a. Impacts of meteoroids larger than 1 m into the Earth's atmosphere. *Astronomy and Astrophysics* 286:967–970.

Ceplecha Z. 1994b. Meteoroid properties from photographic records of meteors and fireballs. IAU Symposium No. 160, Asteroids, Comets, Meteors 1993. p. 343.

Ceplecha Z. 1996. Luminous efficiencies based on photographic observations of Lost-City fireball and implications to the influx of interplanetary bodies onto Earth. *Astronomy and Astrophysics* 311:329–332

Ceplecha Z., Spurný P., Borovička J., and Keclikova J. 1993. Atmospheric fragmentation of meteoroids. *Astronomy and Astrophysics* 279:615–626.

Ceplecha Z., Borovička J., Elford W. G., ReVelle D., Hawkes R. L., Porubčan V., and Šimek M. 1998. Meteor phenomena and bodies. *Space Science Reviews* 84:327–471.

Ceplecha Z., Spalding R. E., Jacobs C., ReVelle D. O., Tagliaferri E.,

and Brown P. 1999. Superbolides. In *Meteoroids 1998,* edited by Baggaley W. J. and Porubčan V. Bratislava: Astronomical Institute and Slovak Academy of Sciences. pp. 37–54.

Christensen P. R. and Moore H. J. 1992. The martian surface layer. In *Mars,* edited by Kieffer H. H., Jakovsky B. M., Snyder C. W., and Matthews M. S. Tucson: University of Arizona Press. pp. 686–729.

Christensen P. R., Bandfield J. L., Clark R. N., Edgett K. S., Hamilton V. E., Hoefen T., Kieffer H. H., Kuzmin R. O., Lane M. D., Malin M. C., Morris R. V., Pearl J. C., Pearson R., Roush T. L., and Ruff S. W. 2000. Detection of crystalline hematite mineralization on Mars by the Thermal Emission Spectrometer: Evidence for near-surface water. *Journal of Geophysical Research* 105:9623–9642.

Chyba C. F. 1993. Explosions of small Spacewatch objects in the Earth's atmosphere. *Nature* 363:701–703.

Chyba C. F., Thomas P. J., and Zahnle K. J. 1993. The 1908 Tunguska explosion: Atmospheric disruption of a stony meteoroid. *Nature* 361:40–44.

Crawford D. A. 1996. Models of fragment penetration and fireball evolution. In *The collision of Comet Shoemaker-Levy 9 with Jupiter,* edited by Noll K. Cambridge: Cambridge University Press. pp. 155–173.

Davis P. M. 1993. Meteoroid impacts as seismic sources on Mars. *Icarus* 105:469–478.

Fadeenko Ju. I. 1967. Disruption of meteor bodies in the atmosphere. *Fizika Gorenija i Vzryva* 2:276–280. In Russian.

Foschini L. 2001. On the atmospheric fragmentation of small asteroids. *Astronomy and Astrophysics* 365:612–621.

Flynn G. J. and McKay D. S. 1990. An assessment of the meteoritic contribution to the martian soil. *Journal of Geophysical Research* 95:14497–14509.

Gault D. E. and Baldwin R. S. 1970. Impact cratering on Mars: Some effects of the atmosphere. *EOS, Transactions, American Geophysical Union* 51:343.

Golub' A. P., Kosarev I. B., Nemtchinov I. V., and Shuvalov V. V. 1996. Emission and ablation of a large meteoroid in the course of its motion through the Earth's atmosphere. *Solar System Research* 30:183–197.

Greeley R., Kuzmin R. O., and Haberle R. M. 2001. Aeolian processes and their effect on understanding the chronology of Mars. *Space Science Reviews* 96:393–404.

Grigorjan S. S. 1979. Motion and disintegration of meteorites in planetary atmospheres. *Kosmicheskie Issledovaniia* 17:724–740. In Russian.

Halliday I., Griffin A. A., and Blackwell A. T. 1981. The Innisfree meteorite fall: A photographic analysis of fragmentation, dynamics, and luminosity. *Meteoritics* 16:153–170.

Halliday I., Griffin A. A., and Blackwell A. T. 1996. Detailed data for 259 fireballs from the Canadian camera network and inferences concerning the influx of large meteoroids. *Meteoritics & Planetary Science* 31:185–217.

Hartmann W. K. 1969. Terrestrial, lunar, and interplanetary rock fragmentation. *Icarus* 10:201.

Hartmann W. K. 1971. Martian cratering III: Theory of crater obliteration. *Icarus* 15:410–428.

Hartmann W. K. and Engel S. 1994. Martian atmospheric interaction with bolides: A test for an ancient dense martian atmosphere (abstract). 25th Lunar and Planetary Science Conference. pp. 511–512.

Hartmann W. K. 1999. Martian cratering VI: Crater count isochrons and evidence for recent volcanism from Mars Global Surveyor. *Meteoritics & Planetary Science* 34:167–177.

Hartmann W. K. and Berman D. C. 2000. Elysium Planitia lava flows: Crater count chronology and geological implications. *Journal of Geophysical Research* 105:15011–15025.

Hartmann W. K., Engel S., Chyba C., and Sagan C. 1994. Mars cratering record as a probe of ancient pressure variations. *Bulletin of the American Astronomical Society* 26:1116.

Hartmann W. K., Malin M., McEwen A., Carr M., Soderblom L., Thomas P., Danielson E. J. P., and Veverka J. 1999. Evidence for recent volcanism on Mars from crater counts. *Nature* 397:586–589.

Hartmann W. K., Anguita J., de la Casa M. A., Berman D. C., and Ryan E. V. 2001. Martian cratering 7: The role of impact gardening. *Icarus* 149:37–53.

Hartmann W. K. and Neukum G. 2001. Cratering chronology and the evolution of Mars. *Space Science Reviews* 96:165–194.

Hills J. G. and Goda M. P. 1993. The fragmentation of small asteroids in the atmosphere. *The Astronomical Journal* 105:1114–1144.

Hildebrand A. R., Brown P. G., Zolensky M. E., Lindstrom D., Wacker J., and Tagliaferri E. 2000. The fireball and strewnfield of the Tagish Lake meteorites, Fell January 18, 2000, in Northern British Columbia. *Meteoritics & Planetary Science* 35:A73.

Hörz F., Cintala M. J., Rochelle W., and Kirk B. 1999. Collisionally processed rocks on Mars: Initial results. *Science* 285:2105–2107.

Ivanov B. A. 2001. Mars/Moon cratering rate ratio estimates. *Space Science Reviews* 96:87–104.

Ivanov B. A., Basilevsky A. T., and Neukum G. 1997. Atmospheric entry of large meteoroids: Implication to Titan. *Planetary and Space Science* 45:993–1007.

Ivanov B. A., Neukum G., and Wagner R. 2001. Size-frequency distributions of planetary impact craters and asteroids. In *Collisional processes in the solar system,* edited by Marov M. Ya. and Rickman H. Dordrecht: Kluwer Academic Publishers. pp. 1–34.

Jenniskens P., Betlem H., Betlem J., Barifaijo E., Schluter T., Hampton C., Laubenstein M., Kunz T., and Heusser G. 1994. The Mbale meteorite shower. *Meteoritics* 29:246–254.

Levin B. I. 1956. Fizicheskaia teoriia meteorov. (Moscow).

Levin B. I. 1961. *Physikalische theorie der meteore und die meteoritische substanz im Sonnensystem.* Berlin: Akademie-Verlag.

Malin M. C. et al. 1998. Early views of the martian surface from the Mars Orbiter Camera of the Mars Global Surveyor. *Science* 279:1681–1692.

Malin M. C. and Edgett K. S. 2000. Sedimentary rocks of early Mars. *Science* 290:1927–1937.

Malin M. C., Caplinger M. A., and Davis S. D. 2001. Observational evidence for an active surface reservoir of solid carbon dioxide on Mars. *Science* 294:2146–2148.

McCord T. B., Morris J., Persing D., Tagliaferri E., Jacobs C., Spalding R., Grady L., and Schmidt R. 1995. Detection of a meteoroid entry into the Earth's atmosphere on February 1, 1994. *Journal of Geophysical Research* 100:3245–3249.

McEwen A. S., Malin M. C., Carr M. H., and Hartmann W. K. 1999. Voluminous volcanism on early Mars revealed in Valles Marineris. *Nature* 397:584–586.

Melosh H. J. 1989. *Impact cratering: A geological process.* New York: Oxford University Press. 253 p.

Murdin P. 2001. *Encyclopedia of astronomy and astrophysics.* London: Nature Publishing Group.

Nemtchinov I. V. and Popova O. P. 1997. An analysis of the 1947 Sikhote-Alin event and a comparison with the phenomenon of February 1, 1994. *Solar System Research* 31:408–420.

Nemtchinov I. V. and Shuvalov V. V. 1992. The explosion in the atmosphere of Mars caused by a high-speed impact of cosmic bodies (abstract). 23rd Lunar and Planetary Science Conference. pp. 981–982.

Nemtchinov I. V., Popova O. P., Shuvalov V. V., and Svetsov V. V. 1994. Radiation emitted during the flight of asteroids and comets through the atmosphere. *Planetary and Space Science* 42:491–506.

Nemtchinov I. V., Popova O. P., and Spalding R. E. 1998. Impacts of 1–10 m in diameter meteoroids onto the surface of Mars (abstract). 29th Lunar and Planetary Science Conference. p. 1272.

Nemtchinov I. V., Svetsov V. V., Kosarev I. B., Golub' A. P., Popova O. P., Shuvalov V. V., Spalding R. E., Jacobs C., and Tagliaferri E. 1997. Assessment of kinetic energy of meteoroids detected by satellite-based light sensors. *Icarus* 130:259–274.

Nemtchinov I. V., Popova O. P., Rybakov V. A., and Shuvalov V. V. 1999a. Initiation of sandstorms due to impacts of the 1–10 m diameter meteoroids onto the surface of Mars (abstract). 5th International Conference of Mars. p. 6081.

Nemtchinov I. V., Popova O. P., and Teterev A. V. 1999b. Penetration of large meteoroids into the atmosphere: Theory and observations. *Journal of Engineering Physics and Thermophysics* 72:1194–1223.

Nemtchinov I. V., Kuzmicheva M. Yu., Shuvalov V. V., Golub' A. P., Popova O. P., Kosarev I. B., and Borovička J. 1999c. Šumava meteoroid—Was it a small comet? In *Evolution and source regions of asteroids and comets, Proceedings of the IAU Colloquium 173,* edited by Svoren J., Pittich E., and Rickman H. Tatranska' Lomnica: Astronomical Institute, Slovak Academy of Sciences. pp. 51–56.

Neukum G. and Ivanov B. 1994. Crater size distributions and impact probabilities on Earth from lunar, terrestrial-planet, and asteroid cratering data. In *Hazards due to comets and asteroids,* edited by Gehrels T. Tucson: University of Arizona Press. pp. 359–416.

Neukum G., Ivanov B., and Hartmann W. 2001. Cratering records in the inner solar system in relation to the lunar reference system. *Space Science Reviews* 96:55–86.

Nyquist L. E., Bogard D. D., Shih C. Y., Greshake A., Stöffler D., and Eugster O. 2001. Ages and geologic histories of martian meteorites. In *Chronology and evolution of Mars,* edited by Kallenbach R., Geiss J., and Hartmann W. K. Bern: International Space Science Institute. pp.105–164.

Pack D. W., Tagliaferri E., Yoo B. B., Peterson G. E., and Spalding R. 1999. Recent satellite observations of large meteor events (abstract). In *Asteroids, comets, meteors 1999.* Ithaca: Cornell University. p. 48.

Padevēt V. 1991. Penetration of chondrites into Mars' atmosphere. *Bulletin of the Astronomical Institutes of Czechoslovakia* 42:206–215.

Passey Q. and Melosh H. J. 1980. Effects of atmospheric breakup on crater field formation. *Icarus* 42:211–213.

Pedersen H., Spalding R., Tagliaferri E., Ceplecha Z., Risbo T., and Haack H. 2001. Greenland superbolide event of 1997 December 9. *Meteoritics & Planetary Science* 36:549–558.

Pollack J. B., Kasting J. F., Richardson S. M., and Poliakoff K. 1987. The case for a wet, warm climate on early Mars. *Icarus* 71:203–224.

Popova O. P. 1997. Determination of parameters of large meteoroids basing on observational data. Ph.D. thesis, IDG RAS, Moscow, Russia. 198 p.

Popova O. P. and Nemtchinov I. V. 1996. Estimates of PN bolide characters of PN bolide characteristics based on the light curves (abstract). *Meteoritics & Planetary Science* 31:A110.

Popova O. P. and Nemtchinov I. V. 2000. Estimates of some recent satellite registered bolides. *Meteoritics & Planetary Science* 35:A129.

Popova O. P. and Nemtchinov I. V. 2002. Strength of large meteoroids entering Earth atmosphere. In *Proceedings of the ACM Conference, Asteroids, Comets, Meteors 2002.* pp. 281–284.

Rybakov V. A., Nemtchinov I. V., Shuvalov V. V., Artemieva V. I., and Medveduk S. A. 1997. Mobilization of dust on the Mars surface by the impact of small cosmic bodies. *Journal of Geophysical Research* 102:9211–9220.

Schmidt R. M. and Housen K. R. 1987. Some recent advances in the scaling of impact and explosion cratering. *International Journal of Impact Engineering* 5:543–560.

Shoemaker E. M. 1965. Preliminary analysis of the fine structure of the lunar surface. Jet Propulsion Laboratory Report 32–700. pp. 75–134.

Strom R. G., Croft S. K., and Barlow N. G. 1992. The martian impact cratering record. In *Mars,* edited by Kieffer H. H., Jakovsky B. M., Snyder C. W., and Matthews M. S. Tucson: University of Arizona Press. pp. 383–423.

Svetsov V. V., Nemtchinov I. V., and Teterev A. V. 1995. Disintegration of large meteoroids in Earth's atmosphere: Theoretical models. *Icarus* 116:131–153.

Tagliaferri E., Spalding R., Jacobs C., Worden C., and Erlich A. 1994. Detection of meteoroid impacts by optical sensors in Earth orbit. In *Hazards due to comets and asteroids,* edited by Gehrels T. Tucson: University of Arizona Press. pp. 199–220.

Tanaka K. L. 1986. The stratigraphy of Mars. J*ournal of Geophysical Research* 91:E139–E158.

Tsvetkov V. I. and Skripnik A. Ya. 1991. Atmospheric fragmentation of meteorites according to the strength theory. *Solar System Research* 25:273–278.

Vasavada A. R., Milavec T. J., and Paige D. A. 1993. Microcraters on Mars: Evidence for past climate variations. *Journal of Geophysical Research* 98:3469–3476.

Ward W. R. 1992. Long-term orbital and spin dynamics of Mars. In *Mars,* edited by Kieffer H., Jakovsky B., Snyder C. W., and Matthews M. S. Tucson: University of Arizona Press. pp. 298–320.

Weibull W. A. 1951. Statistical distribution function of wide applicability. *Journal of Applied Mechanics* 10:140–147.

Zahnle K. J. 1992. Airburst origin of dark shadows on Venus. *Journal of Geophysical Research* 97:10243–10255.